



1
2 **A new multi-resolution bathymetric dataset of the Gulf of Naples (Italy) from**
3 **complementary multi-beam echosounders**

4
5 Federica Foglini¹, Marzia Rovere¹, Renato Tonielli¹, Giorgio Castellan^{1,2*}, Mariacristina Prampolini^{1,2},
6 Francesca Budillon¹, Marco Cuffaro³, Gabriella Di Martino¹, Valentina Grande¹, Sara Innangi¹, Maria
7 Filomena Loreto¹, Leonardo Langone⁴, Fantina Madricardo¹, Alessandra Mercorella¹, Paolo Montagna⁴,
8 Camilla Palmiotto¹, Claudio Pellegrini¹, Antonio Petrizzo¹, Lorenzo Petracchini³, Alessandro Remia¹,
9 Marco Sacchi¹, Daphnie Sanchez Galvez¹, Anna Nora Tasseti⁵, Fabio Trincardi⁶.

10
11 ¹ CNR –ISMAR - National Research Council, Institute of Marine Sciences, Italy;
12 ² NBFC - National Biodiversity Future Centre, Italy
13 ³ CNR-IGAG - National Research Council, Institute of Environmental Geology and Geoenvironment, Italy;
14 ⁴ CNR ISP - National Research Council, Institute of Polar Sciences, Italy;
15 ⁵ CNR IRBIM- National Research Council, Institute for Biological Resources and Marine Biotechnologies, Italy;
16 ⁶ CNR-DSSTTA - National Research Council, Department of Earth Systems Science and Environmental Technologies, Italy.
17 *Correspondence to:* giorgio.castellan@cnr.it

18 **Abstract**

19 High-resolution bathymetry provides critical information to marine geoscientists. Bathymetric big data help characterise the
20 seafloor and its benthic habitats, understand sedimentary records, and support the development of offshore engineering
21 infrastructures. From September 27th to October 20th, 2022, the new CNR Research Vessel GAIA BLU explored the seafloor
22 of the Naples and Pozzuoli Gulfs, and the Amalfi coastal area (Tyrrhenian Sea, Italy) from 50 to more than 2000 m water
23 depth, acquiring about 5000 km² of multi beam echosounder data. This area is particularly vulnerable to abrupt changes driven
24 by the dynamics of several volcanic complexes, active in the area, and by human-induced impacts reflecting the proximity to
25 the highly populated and touristic coastal area of Naples and nearby famous islands. For these reasons, the seafloor of the area
26 needs to be known and constantly monitored. The digital bathymetric data previously available are restricted to the shallow
27 highly dynamic area of the Gulf of Naples and appear fragmented as they were acquired in successive years, with different
28 goals thereby using a variety of devices, with markedly different spatial resolutions. In this paper, we present bathymetric
29 maps of the Gulf of Naples and adjacent slope basins at unprecedented resolution using three state-of-the-art multi beam
30 echosounders. These high-resolution data highlight the technological advances of geophysical surveys achieved over the last
31 20 years and contribute to assessing the most dynamic areas where changes in the seafloor over time can be quantified. The
32 new digital multi-resolution bathymetric products are openly accessible via Marine Geosciences Data System MGDS (refer to



33 section Data Availability, Table 8, for datasets and products DOIs), perfectly matching the FAIR (Findable, Accessible,
34 Interoperable and Reusable) and Open Science Principles.

35 1. Introduction

36 In 2018, GEBCO and the Nippon Foundation joined forces to establish the Nippon Foundation GEBCO Seabed 2030 Project
37 (Mayer et al., 2018), an international effort to foster the complete mapping of the world ocean by 2030. Despite many years
38 of mapping efforts unveiled increasingly larger portions of the seabed, only about 25% of the world oceans seafloor is mapped
39 to date at high resolution (<https://seabed2030.org/our-mission/>). Obtaining a high-resolution map of the world's seafloor is
40 crucial to understanding how oceans work, from geodynamics and geohazards aspects, to the interactions between seafloor
41 morphology and bottom-current dynamics, and to the distribution and ecological status of benthic habitats. In the last 40 years,
42 almost two-thirds of marine environments have been “severely altered” by human activity (Díaz et al., 2019) resulting in
43 significant biodiversity loss and erosion of the ecological services and goods (Worm et al., 2006). In this context, the European
44 Union has implemented a governance framework specifically aiming at assessing, monitoring, and preserving the status of the
45 marine benthic natural heritage (Marine Strategy Framework Directive MSFD, 2014/89/EU), but also at promoting the
46 sustainable exploitation of marine and coastal resources (European MSP Directive, 2008/56/EC). Among the European Seas,
47 the Mediterranean Sea is a hotspot of biodiversity, hosting more than 7.5% of global biodiversity (Bianchi and Morri, 2000)
48 with a high percentage of endemic species (Myers et al., 2000) and unique ecosystems. However, the basin is recognized to
49 be “under siege” due to the historical and still ongoing impacts from multiple stressors such as littering and dumping, trawling,
50 ghost fishing, seaborne traffic and modification of the seafloor (Coll et al., 2012; Puig et al., 2012; Madricardo et al., 2017,
51 2019; Canals et al., 2021; Budillon et al., 2022; Pellegrini et al., 2023; Trincardi et al., 2023). This is particularly evident in
52 the Gulf of Naples, a densely populated coastal region stretching along 385 km on the eastern Tyrrhenian Sea, which represents
53 an important tourist destination including the Gulf Islands (Capri, Ischia and Procida), Sorrento Peninsula, Vesuvius National
54 Park, Phlegraean Fields and archaeological sites of Pompeii, Herculaneum, Pozzuoli and Cuma.

55 The underwater landscape of the Gulf of Naples is geomorphologically complex, with large canyon systems, marine landslides,
56 debris flow deposits, volcanic apparatuses; the area includes various benthic habitats of ecological relevance from the shore to
57 the deep sea, such as *Posidonia oceanica* meadows (e.g., MATTM, 2004), animal forests (e.g., Bavestrello et al., 2014), cold-
58 water corals (CWC, Taviani et al., 2019; Angiolillo et al., 2023), and hydrothermal vent communities (e.g. Apolloni et al.,
59 2020; Donnarumma et al., 2019). The gulf region also hosts numerous archaeological and cultural heritage sites, threatened
60 by natural and human pressures (Mattei et al. 2019). To preserve marine biodiversity and the historical value of the area, four
61 Marine Protected Areas (MPAs) have been established: the Underwater Parks of Baia and Gaiola MPAs, the Regno di Nettuno
62 MPA and the Punta Campanella MPA (Apolloni et al., 2018).

63 The first extensive high-resolution mapping of the seafloor of the gulf was performed in the framework of the Italian geological
64 mapping research program (1997-2017), through bathymetric surveys of the continental shelf/slope system of the Campania



65 region using numerous multi beam echosounder systems (MBESs) with an average vertical resolution of < 0.25% of the water
66 depth and position accuracy better than 10 m. The data, acquired at different resolutions, were merged to create a Digital
67 Terrain Model (DTM) with a homogeneous grid and with a cell spacing of 20 m (Aiello et al., 2020). This map highlighted
68 the most prominent geomorphological features in the coastal zone such as the canyons, banks, debris avalanches, hydrothermal
69 vents and volcanoclastic basement outcrops with high ecological value habitats in urgent need of preservation (Taviani et al
70 2019). This valuable dataset was shared in gridded form, within the EMODnet project, as 1/16 arc minutes (ca. 115 m) DTMs.
71 High-resolution data for selected areas are also available as 1/128 or 1/256 arc minutes (ca.15 m or 7 m) HR-DTMs
72 (<https://emodnet.ec.europa.eu/geoviewer/>).

73 Despite the significant effort of ongoing national and international projects and infrastructures worldwide to make data
74 available, such as GEBCO (<https://www.gebco.net>) and EMODnet (<https://emodnet.ec.europa.eu/en>), local high-resolution
75 datasets and raw data are typically not yet accessible (Sievers et al., 2021). Indeed, databases are often generated, hosted, and
76 administered by various institutes in the world with dissimilar data policies, which often do not follow the Findable, Accessible,
77 Interoperable and Reusable (FAIR) data principles (Stall et al., 2019).

78 This study presents the results of a high-resolution geophysical survey conducted in October 2022 on board R/V Gaia Blu
79 using three different state-of-the-art MBESs (Kongsberg EM 2040, EM 712, and EM 304) and aims at improving the
80 knowledge of the seascape of the Gulf of Naples by enhancing the analysis/visualization of seabed morphology through high-
81 resolution digital bathymetric models.

82 Given the unprecedented high- and multi-resolution survey conducted in the study area and the availability of ancillary data
83 such as backscatter and water-column data, this dataset represents a unique benchmark for future studies related to geohazards
84 assessment, sediment transport, fishery management, resource exploration and sustainable exploitation, maritime spatial
85 planning and decision making, marine ecosystem and habitat mapping, oceanographic modeling including storm surges and
86 scenarios of tsunami wave propagation.

87 We discuss the quality of the data collection (section Data Quality) and present three examples that highlight the potential
88 applications of this dataset (Section Results and discussion). Our contribution also aims at highlighting the innovative approach
89 used during JammeGaia22 (Section Multibeam data processing), where data are processed daily on board and can be made
90 available to the scientific community and the generic public in near real-time via a geoportal, making the datasets FAIR and
91 facilitating interdisciplinary research within the Open Science Principles.

92

93 **2 Study area - Geological and geomorphological background**

94 The investigated area belongs to the central-eastern margin of the Tyrrhenian Sea, encompassing the region between the



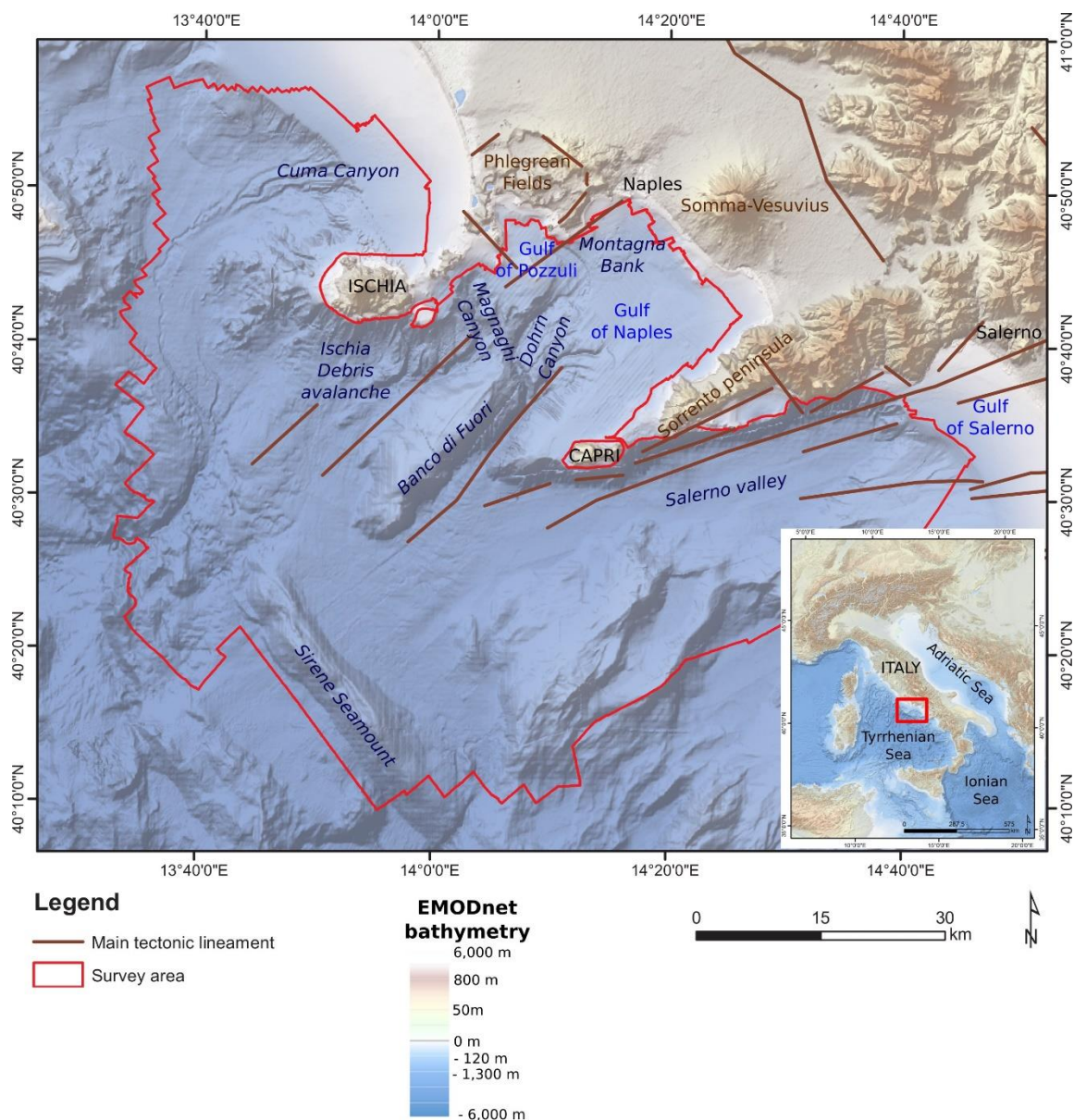
95 western margin of the Southern Apennines thrust belt and the Tyrrhenian abyssal plain (ca.3000 m deep; Figure 1). The
96 Tyrrhenian Sea is the youngest back-arc basin of the Mediterranean Sea that developed since the Middle Miocene (Trincardi
97 and Zitellini, 1987; Kastens et al., 1988; Lymer et al., 2018; Loreto et al., 2021; Miramontes et al., 2023) reflecting the east-
98 and south-eastward retreat of the Ionian slab, guided by the Africa-Europe convergence (Moussat et al., 1985; Malinverno and
99 Ryan, 1986; Kastens et al., 1988). The Campania segment of the eastern Tyrrhenian margin is characterized by a series of NE-
100 SW trending half-graben bounded by structural highs that have developed since the early Pleistocene and accommodate the
101 tectonic-controlled subsidence of the alluvial plains along with their submerged counterparts, namely the Gaeta Gulf, the Gulf
102 of Naples and the Gulf of Salerno (Figure 1; Romano et al., 1984; Ruberti et al., 2022; Amato et al., 2011; Bellucci et al.,
103 2006).

104 Structural lineaments also control the preferential pathways of volcanic activity, particularly in the last 2 My. Volcanic activity
105 followed an eastward migration, governing the geomorphological setting of the region and promoting deposition of
106 sedimentary sequences up to 3 km thick (Milia, 1999; Milia et al., 2003). The Phlegraean Fields volcanic area is a 78-ka old
107 active poly-calderic system (Scarpati et al., 2012) that has affected its territory in the last millennia and has strongly influenced
108 the evolution of the adjacent coasts during the late Pleistocene and Holocene, which has been mainly shaped by three super-
109 eruptions. The oldest one was the Campanian Ignimbrite (CI) eruption that occurred at ca. 35-40 ka BP (Giaccio et al., 2017).
110 After this main event, the northern part of the just-formed caldera was submerged by the sea. The second eruption, which led
111 to the formation of the Masseria Del Monte Tuff, occurred at 29.3 ka BP (Albert et al., 2019). The Neapolitan Yellow Tuff
112 (NYT; Deino et al. 2004) eruption at ca. 15 ka BP contributed to the formation of the youngest caldera (Orsi et al., 1992),
113 nowadays well documented also offshore (Sacchi et al., 2014; Steinmann et al., 2016, 2018). Besides volcanic eruptions,
114 alternating long-term magma/hydrothermal fluid inflation and deflation processes controlled the morphological evolution of
115 this area. Further, short-term vertical, meter-scale, ground movements characterised times immediately preceding and
116 following each eruption, which produced rapid relative sea-level variations along the entire coastal sector (Isaia et al., 2019
117 and reference therein). The area has experienced high rates of subsidence (approx. 4.0 mm/yr) through the Pleistocene
118 (Torrente et al., 2010; Milia et al., 2017; Iannace et al., 2018), accompanied by the activity of major NE-SW-striking faults.
119 At present, intense seismicity, including the Md 4.0 earthquake occurred on 2nd October 2023, is instead associated to the
120 18.0 mm/yr uplift of the central portion of the Phlegraean Field area.

121 Volcanic activity, long-term vertical ground movements, glacio-eustasy and the rapid dismantling of the emerging landscapes
122 have driven a rapid geomorphological evolution of the margin, resulting in steep slopes, canyoning, deep-sea fan accretion and
123 gravitational slope instability. Extensive lateral collapses of the volcanic edifices have been documented offshore, south of
124 Ischia Island (Chiocci et al., 1998; Chiocci and de Alteriis, 2006; de Alteriis et al., 2010), possibly occurred also in historical
125 time, and two others of minor extent to the west and north of Ischia Island (Budillon et al., 2003; Violante et al., 2003) and in
126 the Gulf of Naples (Milia et al., 2008, 2012; Passaro et al., 2018). The rapid aggradation of volcanoclastic deposits in shallow
127 marine environment and the entrance of pyroclastic flows into the seawater also led to seafloor instability and creep in the
128 prodelta offshore the main rivers (Sacchi et al., 2005; 2009).



129 Three main turbiditic systems, namely Cuma, Magnaghi and Dohrn Canyons, and the deep structurally controlled Salerno
130 Valley, have developed along with the rising of intra-slope reliefs and volcanic activity, and acted as main conduits delivering
131 sediment towards deeper-water domains (Passaro et al., 2016). These features characterize the present-day seafloor
132 morphology and, although partially inactive, are of paramount interest as hotspots of biodiversity in the Mediterranean Sea
133 (e.g., Taviani et al., 2019; Mussi et al., 2022).



134
135
136
137

Figure 1. Map of the study area in the central Tyrrhenian Sea showing the main physiographic and tectonic features (modified from Aiello et al., 2020). Elevation and bathymetry from EMODnet bathymetry (<https://emodnet.ec.europa.eu/en/bathymetry>).



138 3. Materials and methods

139 3.1 Multi beam data acquisition

140 Multi beam data were collected during the JammeGaia22 cruise from September 27th to October 20th 2022 using three different
141 MBES: the Kongsberg EM2040-04 MKII 0.4°x0.7° suited for water depths between 50 and 150 m, Kongsberg EM712 1°x0.5°
142 for water depths between 150 and 1000 m and Kongsberg EM304 MKII 1°x1° for water depth greater than 1000 m (Table
143 1 for acquisition settings).

144 Table 1. Acquisition settings for the three multi beam echosounder systems.

MBES	Water depth (m)	Frequency (kHz)	Angular coverage (degree)	Ping rate (Hz)	Acquisition mode
EM2040	50-100	300	65	1.5	Deep
EM2040	100-150	200	70	1.5	Very deep
EM712	150-600	70-100	70	2	Shallow
EM712	600-1000	40-100	70	2	Deep
EM304	>1000	30	65	>5	Auto

145

146 The MBESs were hull-mounted on the R/V GAIA BLU gondola with a T-configuration of linear transducer arrays. A Seapath
147 380 system was used for ship positioning, supplied by a Fugro HP differential Global Positioning System (DGPS), with
148 Marinestar GNSS signal accuracy better than 5 cm. The Kongsberg motion sensor MRU (Motion Reference Unit) 5 and a Dual
149 Antenna GPS integrated into the Seapath, were used to correct for pitch, roll, heave and yaw movements (reaching 0.02° roll
150 and pitch accuracy, and 0.075° heading accuracy). A Valeport mini SVS sensor was positioned close to the transducers to
151 continuously measure the sound velocity for the beamforming. Sound velocity profiles (SVPs) were systematically collected
152 at least twice a day with a Valeport Midas SVP, for a total of 40 SVPs. Data were logged, displayed and checked in real-time
153 by the Kongsberg data acquisition and control software SIS 5 (Seafloor Information System). A software tool was used to
154 extend the SVPs down to 1200 m water depth. Since the Mediterranean Sea is characterized by a stratified water column with
155 peculiar changes in the physical-chemical properties (Tanhua et al. 2013; Rossi et al. 2014; Basterretxea et al. 2018), a linear
156 regression based on the collected SVP data was run in R software (R Core Team, 2019) to estimate the sound velocity values
157 down to 12000 m depth.

158

159 Professional topographers measured the offsets of the instruments with millimetric accuracy using a dedicated dimensional
160 survey of the ship's hull at dry dock.

161 Sensors have been calibrated during the Sea Acceptance Tests (roll, pitch, time and heading offsets) and were also regularly
162 checked in post-processing (Table 2 for calibration values).



Table 2. Calibration values applied after the Sea Acceptance Test.

MBES	Pitch	Roll	Heading
EM2040	+0.10°	+0.5°	-0.20°
EM304	00.00°	+0.2°	0.00°
EM712	-0.10°	-0.07°	-0.15°

163

164

165 We kept a 20% overlap between lines, avoiding the influence of external beams of bad quality given by possible residual errors
166 in roll and sound speed profile measurements. The multi beam operated with an average swath opening angle of about 65°/70°
167 (Table 1) for each multi beam system. The vessel sailed with a reasonably constant speed of 8 knots, considered ideal to have
168 the minimum noise and tested during the Sea Acceptance Test. Seafloor and water column backscatter data were collected
169 simultaneously during bathymetric data acquisition.

170

171 **3.2 Multibeam data processing**

172 The bathymetric data collected were immediately processed on-board to produce DTMs and backscatter mosaics, uploaded
173 daily in a dedicated WebGIS to inform the scientific community on the progress of the campaign and make the data openly
174 available. The data processing workflow is summarized in Figure 2.

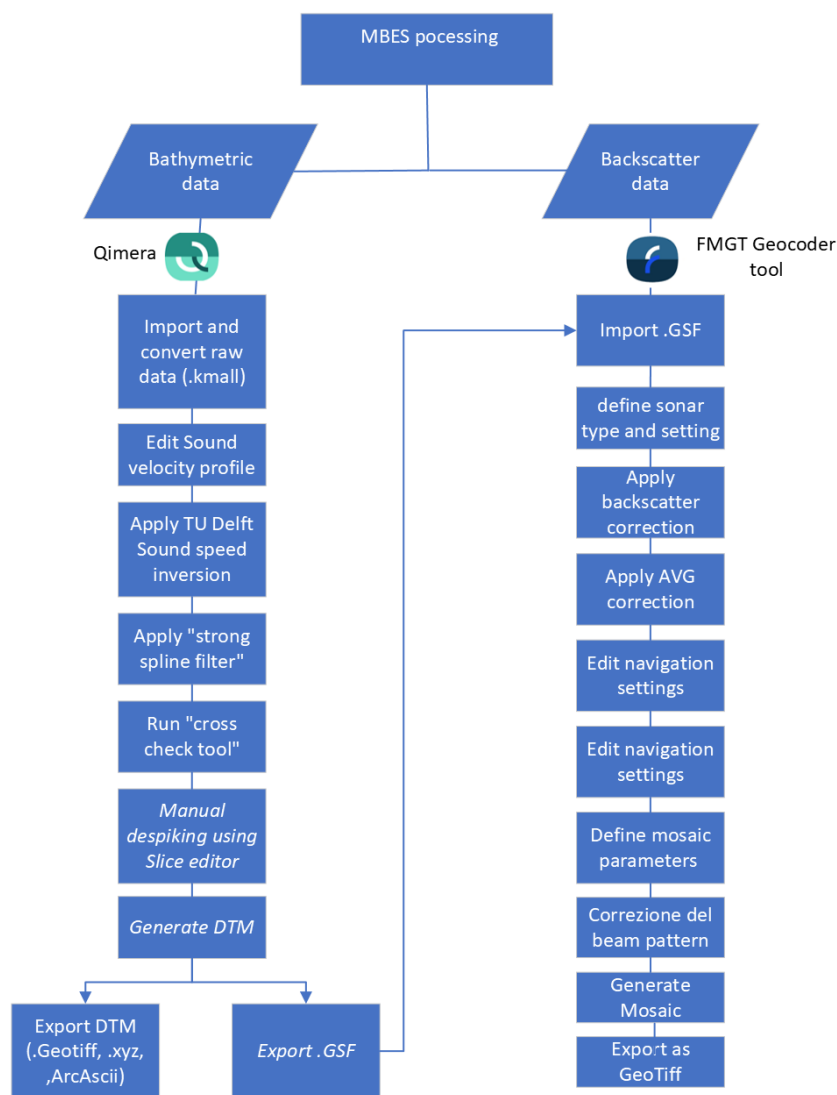


Figure 2. Workflow of bathymetric and backscatter data processing.

175
176
177

178 3.2.1 Bathymetric data processing

179 The processing of the raw data was carried out using the QPS Qimera v.2.5.0 software (Quality Positioning Services BV, Zeist,
180 Netherlands) following a standard procedure, which includes sound speed correction, removal of erroneous soundings, and
181 correction of vertical offsets. The quality of the data was initially checked using the ‘Cross Check Tool’ to check for soundings
182 with significant offsets from the local mean water depth.



183 When sound velocity errors were evident in the data, the TU Delft Sound Speed Inversion tool (Beaudoin et al., 2018) was
 184 used to correct the profile. The tool applies an algorithm that allows a completely automated refraction error correction. It
 185 works by taking advantage of the overlap between survey lines to simultaneously estimate sound speed correction for a given
 186 set of pings and their neighbours, by computing a best-fit solution that minimizes the mismatch in the areas of overlap between
 187 lines (Mohammadloo et al., 2019). The settings applied for TU Delft Sound Inversion were data-specific, depending on the
 188 quality of the SVP, upon initial assessment. Nevertheless, we typically applied the ‘Quick Search’ algorithm and ‘Coarse’
 189 configuration as an initial setting, and we then applied adjustments if necessary.

190 After the sound speed correction, the strong spline filter of Qimera allowed removal of soundings beyond the local mean water
 191 depth (offsets); the remaining offsets (if any) were removed manually using the ‘Slice editor’ of Qimera. The processed
 192 bathymetric data were exported into GSF format for backscatter processing and to a gridded surface data (GeoTIFF). The
 193 resolution of the GeoTIFF was defined based on the water depth and the footprint calculated for each sonar used (Table 3).

194

195 Table 3. Calculated footprints of ensonified seafloor area at different water depths for each MBES. Products and dataset are available at
 196 section Data Availability.

MBES	Water Depth (m)	TX Footprint (m)	RX Footprint (m)	Insonified area (mq)	Grid resolution (m)
EM2040 (0.4°x 0.7°)	50	0.4363	0.6109	0.92	2
	60	0.5236	0.7330	1.10	
	70	0.6109	0.8552	1.28	
	80	0.6981	0.9774	1.46	
	90	0.7854	1.0996	1.65	
	100	0.8727	1.2217	1.83	
EM712 (0.5°X1°)	150	1.3090	2.6181	3.28	5
	200	1.7453	3.4907	4.37	
	300	2.6180	5.2361	6.56	
	400	3.4907	6.9815	8.75	10
	500	4.3634	8.7269	10.94	
	600	5.2360	10.4722	13.12	15
	700	6.1087	12.2176	15.31	
	800	6.9814	13.9630	17.50	20
	900	7.8540	15.7084	19.69	
	1000	8.7267	17.4537	21.87	



EM304 (1°X1°)	1000	17.4537	17.4537	30.94	30
	1100	19.1991	19.1991	34.03	
	1200	20.9445	20.9445	37.12	
	1300	22.6899	22.6899	40.22	40
	1400	24.4352	24.4352	43.31	
	1500	26.1806	26.1806	46.40	
	1600	27.9260	27.9260	49.50	
	1700	29.6714	29.6714	52.59	
	1800	31.4167	31.4167	55.68	
	1900	33.1621	33.1621	58.78	
	2000	34.9075	34.9075	61.87	

197

198

199 3.2.2 Backscatter data post-processing

200 The MBES backscatter data were processed using the QPS Fledermaus Geocoder Tool (FMGT) v.7.10.2 software. The
 201 processed MBES data (.gsf) were used to apply backscatter corrections, beam pattern correction, and angle-varying gain
 202 (AVG) corrections to the backscatter data. After these corrections, FMGT applied the sonar’s navigation data (i.e., XY
 203 coordinates, roll, heading, pitch, heave) to improve the spatial accuracy of the data. The DTM generated in Qimera provided
 204 a reference grid to improve backscatter corrections. The reference grid was included by the FMGT software to determine
 205 topographic slope, while the corrected bathymetry in the source files (i.e., GSF) was regularly used to geo-reference the snippet
 206 trace from a single ping to the correct spot on the seafloor and with the correct scaling (Quality Positioning Services B.V.,
 207 2020). Finally, the backscatter snippets were mosaicked with the ‘No Nadir possible, 25% overlap’ algorithm to reduce the
 208 banding effect, and 30-40% line blending was applied to blend the pixels in the overlapping areas. The mosaics were gridded
 209 in various resolutions (Table 4) with dB values cropped to $\pm 3\sigma$ and logarithmically mapped to 8-bit scale. These mosaics were
 210 exported as ‘One merged Colored GeoTIFF format’.

211

212

Table 4. Resolution of backscatter mosaic for each MBES. Products and dataset are available at section Data Availability.

MBES	Mosaic resolution (m)
EM2040	5 m
EM712	10 m
EM304	30 m



213

214 **3.3 Bathymetric derivatives**

215 A geomorphometric analysis of the seabed was carried out using ArcGIS to emphasize any subtle variation in seafloor
216 morphology. The geomorphometric indices calculated were slope, broad-scale and fine-scale Bathymetric Position Index
217 (BPI), and rugosity.

218 The slope is a first-order derivative of the bathymetry and represents seabed maximum inclination (in any direction) in degrees,
219 using the AreaSlope algorithm, included in Marine Toolbox for ESRI ArcGIS developed by Dr Tim Le Bas (Le Bas 2016),
220 picking an area of 3x3 pixels around each cell. Values are real numbers between 0.0° and 90.0°, areas of no data have a
221 conventional value of -1.0. Depth values in input were smoothed before calculation of the slope using a user-defined smoothing
222 window of 3x3. This approach served to removed local changes giving a regional value for slope and diminishing edge effect
223 (Dolan, 2012).

224 Broad- and fine-scale BPIs were calculated using Benthic Terrain Modeler (BTM) toolbox for ArcGIS (Walbridge et al., 2018;
225 Lundblad et al., 2006). BPI is a second-order derivative (as it is derived from the slope) of the bathymetry and is modified
226 from topographic position index as defined by Weiss (2001) and Iampietro and Kvitek (2002). It evaluates differences in
227 elevation between a focal point and the mean elevation of the surrounding cells within a user-defined window. Values range
228 from -1 to +1, with negative values reflecting depressions in the seabed, null values for planar areas and positive values
229 denoting the reliefs. Broad-scale BPI allows the identification of main regional features within the seafloor, while fine-scale
230 BPI helps identify smaller features of the benthic landscape. The values used to calculate BPIs for all the bathymetric surfaces
231 are reported in Table 5.

232 **4. Results and Discussion**

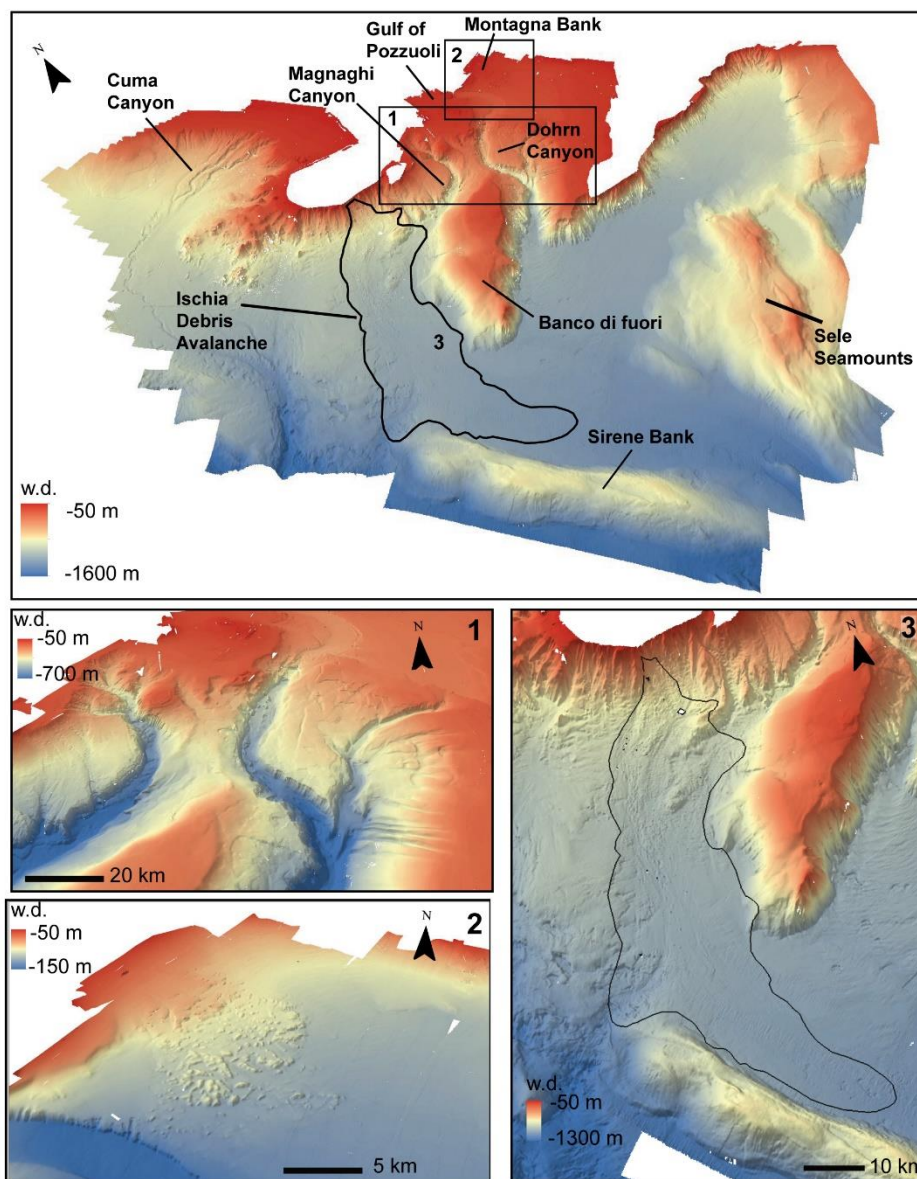
233 **4.1 Multi-resolution bathymetric grid**

234 The multi-resolution grid covers an area of about 5000 km² offshore the Gulf of Naples from 50 to more than 2000 m water
235 depth (Figure 3). The different resolutions, depending on the water depth and the MBES footprint, of the acquired data reveal
236 the complexity of the seafloor with unprecedented details and allow to better discriminate geomorphological features already
237 described in the literature (D'Argenio et al., 2004).

238



239



240

241 Figure 3. Bathymetric map of the study area (20 m resolution, 2 vertical exaggeration) showing the main seabed features; (1) multibeam
242 bathymetry (20 m resolution, 2 vertical exaggeration) of the Dohrn and Magnaghi canyon systems; (2) multibeam bathymetry of the
243 Montagna Bank area; and (3) multibeam bathymetry of the debris avalanche offshore the Ischia Island.

244 Coupled with other indices, this high-resolution bathymetry not only is valuable information to study sediment dynamics, and
245 morphotectonics of canyons, structural highs and seamounts, but also represents a baseline to investigate the presence and
246 distribution of benthic habitats and infer hydrological transients hugging the sea floor. To demonstrate how the newly acquired



247 data allow to appreciate the variations of the seafloor, broad- and fine-scale BPI were calculated from the bathymetry in three
 248 selected sectors of the study area using the parameters reported in Table 5.

249

250 Table 5. Inner and outer radius used for calculation of Bathymetric Position Index (BPI) for selected areas by depth range.

Area	Depth range (m)	Resolution (m)	Broad-scale BPI Inner – outer radius (cells)	Fine-scale BPI Inner – outer radius (cells)
Canyons of the Gulf of Naples	50-100	2	30-60	2-5
	101-200	5	12-30	2-5
	201-500	10	6-15	2-5
	501-700	15	4-9	2-5
	701-1000	20	3-8	2-5
	1001-2500	30	2-5	2-5
Montagna Bank	50-100	2	30-60	5-8
	101-200	5	12-30	5-8
	201-500	10	6-15	5-8
Ischia debris avalanche	50-100	2	30-60	1-3
	101-200	5	12-30	1-3
	201-500	10	6-15	1-3
	501-700	15	4-9	1-3
	701-1000	20	3-8	1-3
	1001-1900	30	2-5	1-3

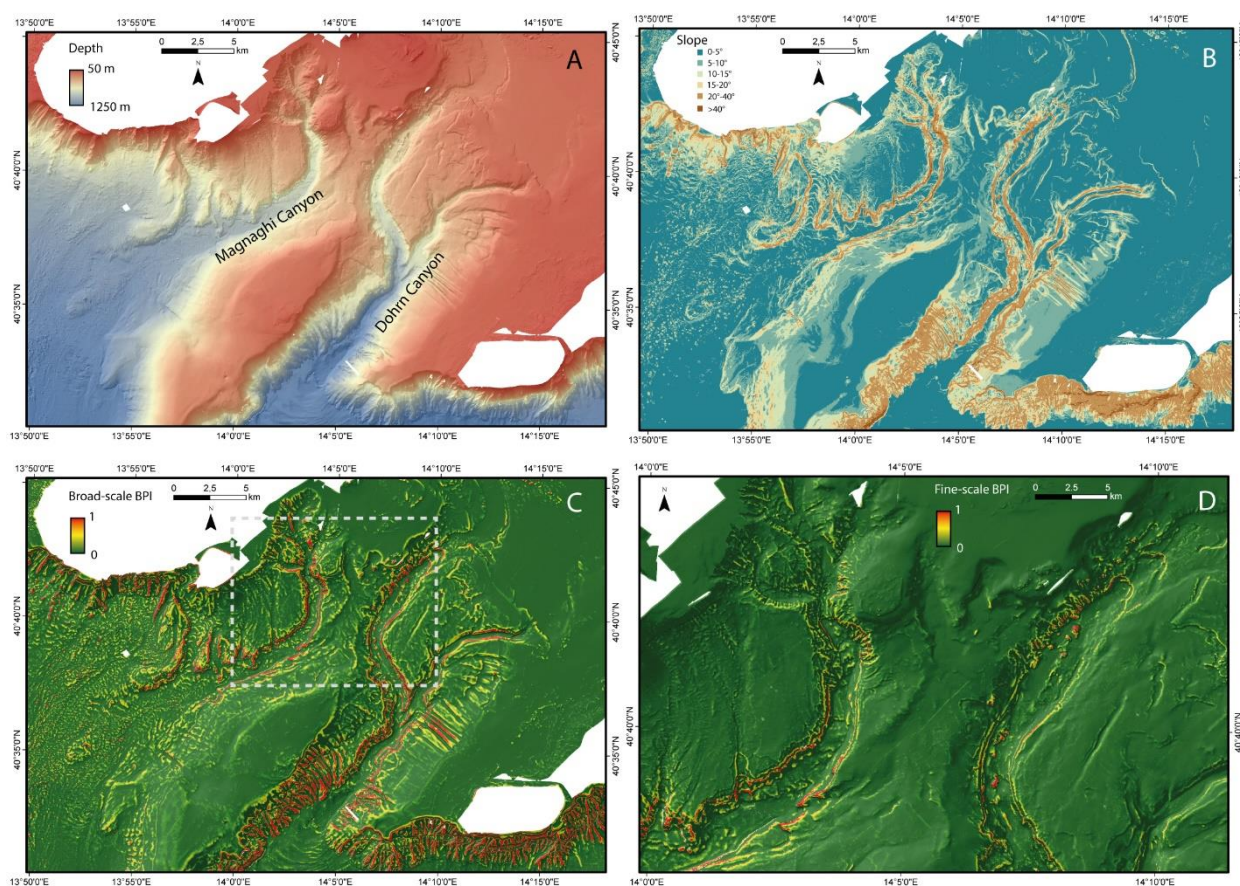
251

252 4.1.1 Canyons of the Gulf of Naples

253 The morphology of the Dohrn and Magnaghi Canyons is possibly controlled by the presence of extensional faults coupled
 254 with the volcanic activity characterising the area. Both canyons acted as large drainage systems within this proximal marine
 255 area during the Late Quaternary (Aiello et al., 2020 and references therein). The two branches of Dohrn Canyon are about 500
 256 m wide and show a V-shaped profile in the upper part and a U-shaped profile in the lower part, suggesting uniform sediment
 257 fill of the thalweg. The bathymetric derivatives confirm the complexity of these drainage patterns showing some differences
 258 possibly related to the stratigraphy of the eroded terrains and to the recurrence and or competence of the flows flushing the
 259 two systems: straight gullies characterise the flanks of Dohrn Canyon and normally do not indent the outer shelf, with the
 260 exception of the area NW of Capri (Fig. 4). Canyon Dohrn emanates from Ammontatura channel, on the inner shelf, a possibly
 261 active sediment conduit also during sea level rise and high stand conditions; Dohrn Canyon undercuts its secondary branch



262 located north of Capri Island under-excavating its base by 50m. The straight gullies on the flanks of Dohrn Canyon are hanging
263 above the canyon thalweg suggesting the activity of powerful flows along the axis of the canyon. Moreover, the fine-scale BPI
264 highlights terrace rims along Dohrn Canyon flanks and slide scars with a slide deposit at their foot (Aiello et al., 2020), as well
265 as the gullies with head scarps and along-slope small-scale sand splays located on the southern flank of Banco di Fuori. Dohrn
266 Canyon shows a radial bedform field in its lower portion where the canyon broadens, and its floor decreases its gradient.
267 Comparison with pre-existing data in this area suggests that the bedform field has not moved in the last two decades.
268 In contrast, Magnaghi Canyon is shorter, less deeply incised and not gullied on its flanks, possibly reflecting its lack of
269 connection to a major source of sediment-laden flows. The right-hand side of the canyon shows short and straight incisions
270 with marked bedforms that appear reminiscent of cyclic steps (Kostic, 2011; Slooman and Cartigny, 2020) and can be clearly
271 discerned on the slope map and on the DPI maps.
272



273
274 Figure 4 (A) Bathymetric data of canyons of the Gulf of Naples; (B) Slope; (C) positive values of broad-scale and (D) fine-scale BPI of a
275 portion of the area (dashed rectangle in C) calculated from the newly acquired multi-resolution grid, showing the drainage pattern of the
276 Dohrn and Magnaghi canyons.



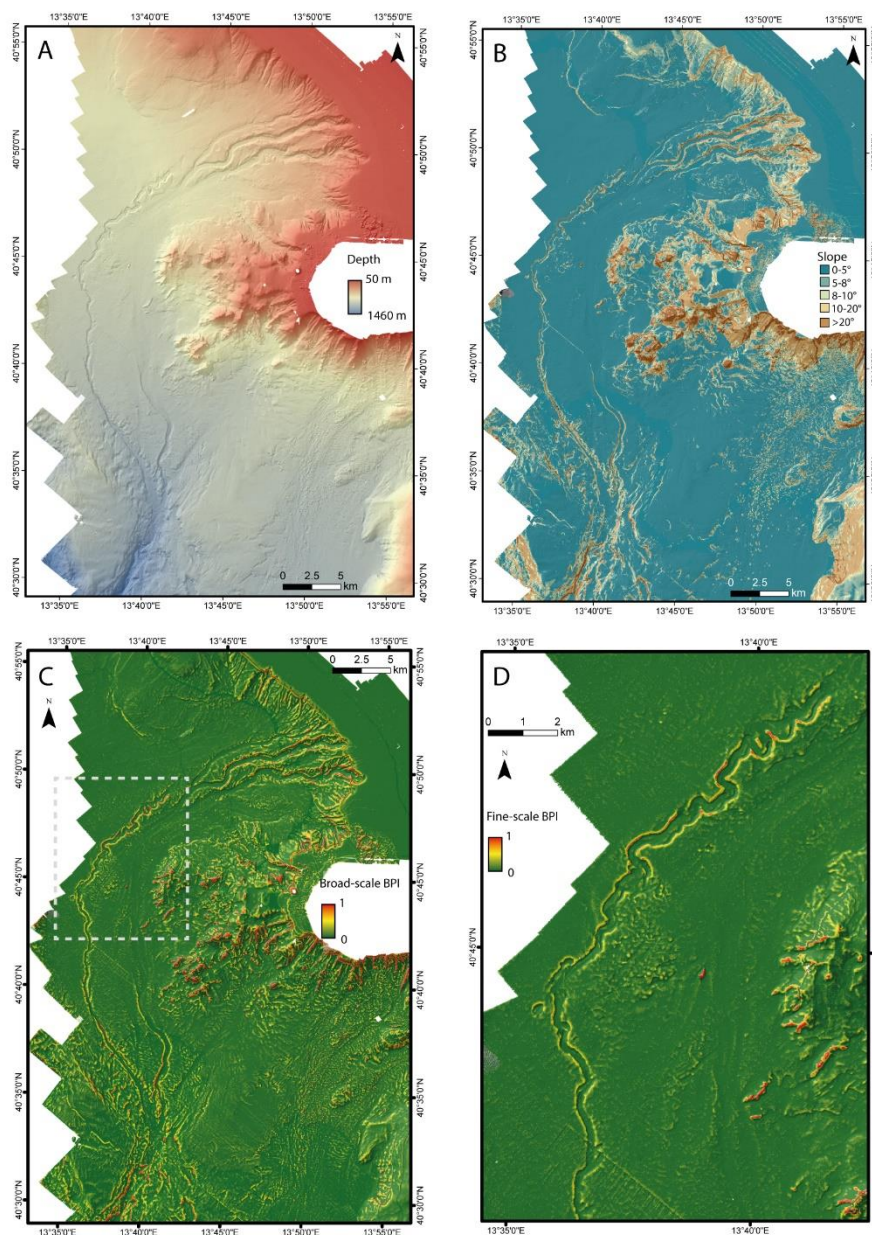
277 **4.1.2 Cuma Channel**

278 Cuma Channel is a complex sediment conduit characterized by 1) an upper section, between the shelf-edge and the base of
279 Gaeta basin, where three independent sub parallel channels present gullied heads, low sinuosity and flat channel floor; 2) a
280 relatively narrow thalweg characterize by a prominent high sinuosity on the sub-horizontal floor of Gaeta Basin and 3) a
281 straighter channel, proceeding in deeper waters across the steepening slope region.

282 Peering both bathymetric and backscatter images prompt several questions that will be worth addressing in future cruises, after
283 collecting complementary core and seismic-stratigraphy data. In particular:

- 284 1) there is no continuity between either of the three channels dissecting the upper slope and the high sinuosity channel
285 on the floor of Gaeta basin; however, backscatter images hint to a seaward continuity of the most meridional of the
286 three slope channels characterized by higher backscatter and, likely, coarser grained sediment. This channel reaches
287 a north-south orientation before widening and rapidly reducing its seafloor reflectivity;
- 288 2) the high sinuosity to the west is therefore disconnected from its original feeder, upslope, and, proceeding downslope,
289 bends gently to the Southeast and then to the Southwest in the lowermost tip of the mapped area; interestingly, the
290 region located west of this gentle, multi-kilometric, bend is carved by several barchan-like scours that can be
291 hypothetically ascribed to overflows of a much larger volume compared to the size of the channel conduit;
- 292 3) knowing that the Volturno prodelta has reached the shelf edge, it is possible that hyperpycnal flows from the river
293 ignite flows on the slope that are capable to hug the seafloor and reshape its morphology, as documented during the
294 modern sea level high stand in some other example of high discharge systems like the Crati River (Lucchi et al.,
295 1983).

296



297

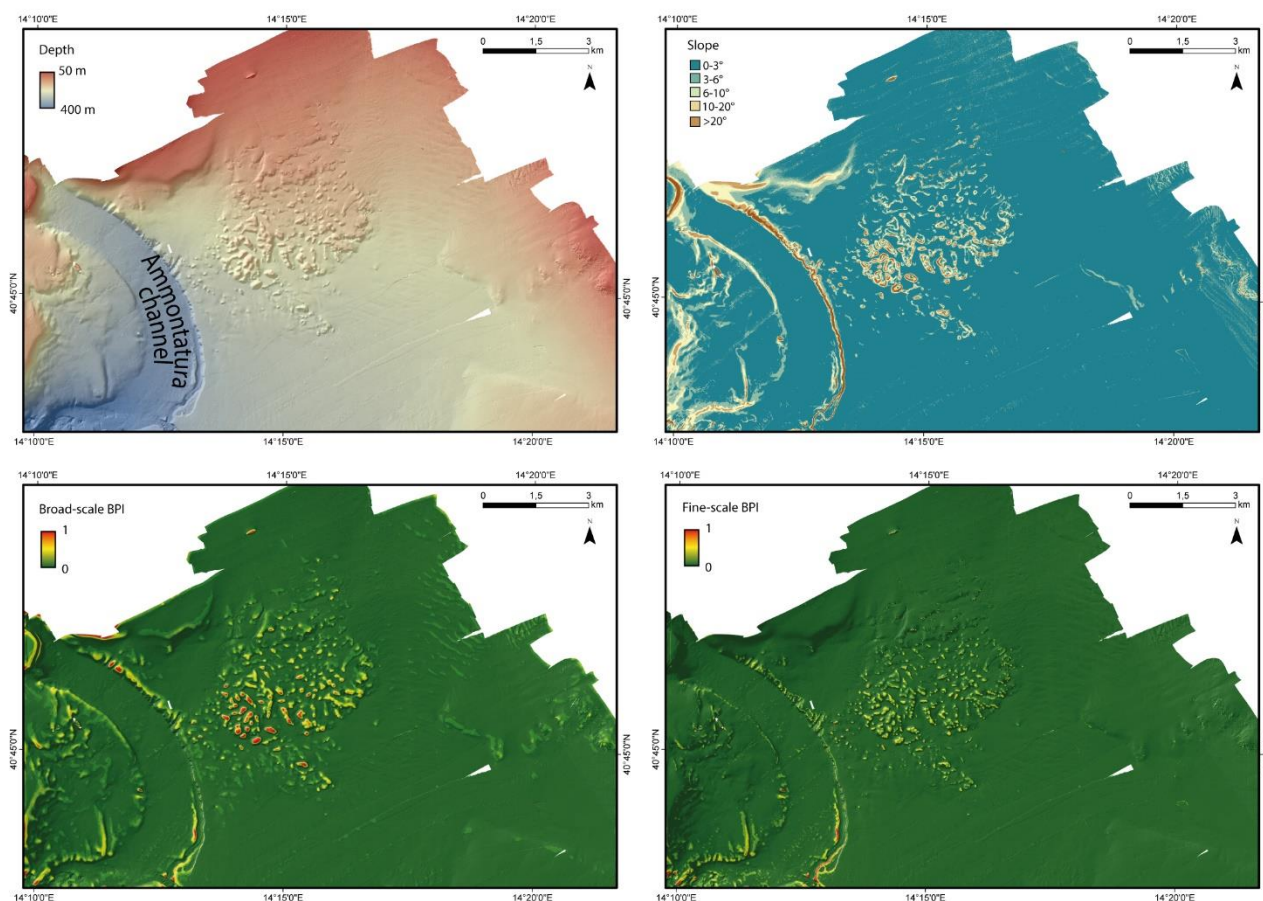
298 Figure 5 (A) Bathymetric data of the Cuma channel; (B) Slope; (C) positive values of broad-scale and (D) fine-scale BPI of a portion of
299 the area (dashed rectangle in C) calculated from the newly acquired multi-resolution grid.

300 4.1.3 Montagna Bank

301 In the shallower area of the Gulf of Naples, **Montagna Bank** is a morphological high extending over 25 km² (Passaro et al.
302 2014, 2016, 2018; Ventura et al. 2016), where volcanoclastic materials (dominantly low-density pumice) underwent small-
303 scale deformation leading to the growth of meter-scale sediment-diapirs and possible fluid-escape features; in particular, this



304 hummocky area includes 280 mounds, 650 cones with meter-scale height, and 30 pockmarks (Sacchi et al., 2019), between
305 100 and 150 m water depth. The slope calculated for the Montagna Bank shows the inclinations of both the whole
306 morphological high and of the individual bedforms surrounding it (i.e., the flanks of the Ammontatura channel and sedimentary
307 bedforms located W of the Montagna Bank). Furthermore, the calculated BPIs reveal large and small mounds constituting the
308 hummocky-like morphology of the large-scale relief.
309



310

311

312

Figure 6. (A) Bathymetric data of the Montagna Bank; (B) Slope; (C) broad-scale and (D) fine-scale BPI calculated from the newly acquired multi-resolution grid, showing the morphology of the Montagna Bank.

313

314

315 4.1.4 Ischia debris avalanche

316

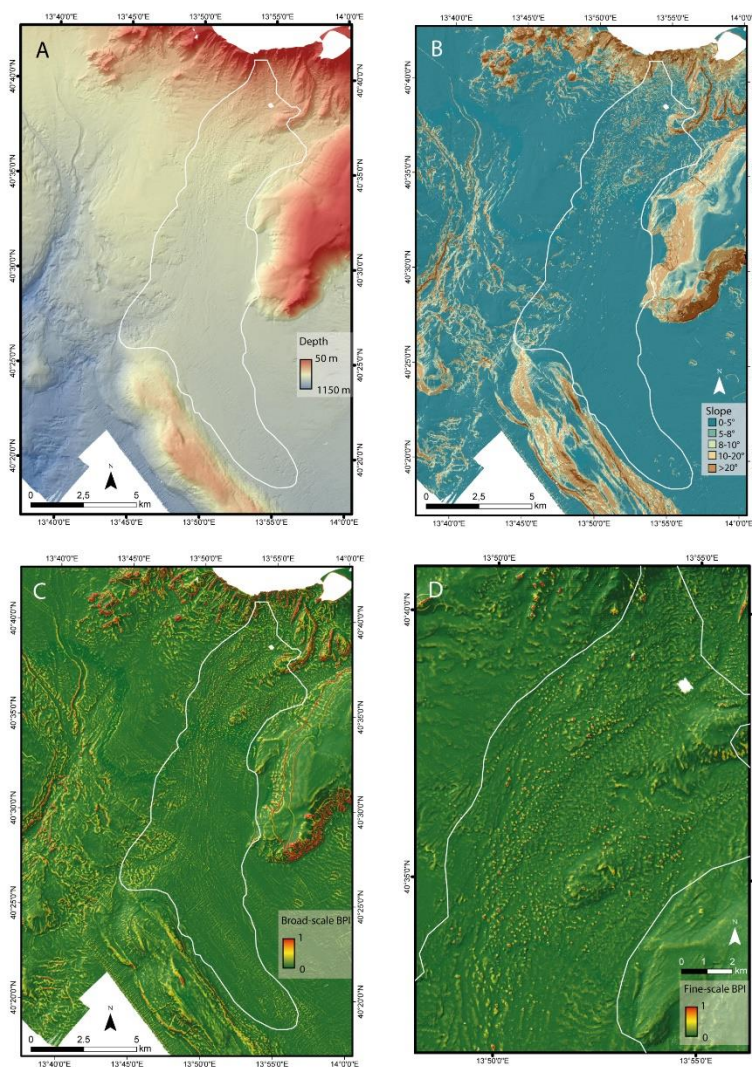
317

318

The Ischia debris-avalanche is located south of Ischia Island and is a 50-km-long tongue characterised by a hummocky topography extending for about 200 km² with fields of giant blocks spanning in size from a few metres to > 200 m across and with larger blocks being up to 30–50 m high (Chiocci and de Alteriis, 2006; de Alteriis et al., 2010). The hummocky deposit



319 follows the local pre-collapse topography, and, on its eastern side, it overflows into the Magnaghi Canyon. The slope (Fig.
320 6B), the broad-scale (Fig. 6C), and fine-scale (Fig. 6D) BPI obtained using different inner and outer rays (Tab. 5), calculated
321 from the newly acquired bathymetric data, allow to better appreciate the morphology of the deposits and clearly identify
322 individual debris blocks, allowing better measurement of their size and volume.
323



324
325 Figure 7. (A) Bathymetric data of the Ischia Debris Avalanche; (B) Slope; (C) broad-scale and (D) fine-scale BPI calculated from the
326 newly acquired multi-resolution grid, showing the location and morphology of debris blocks. The white square delimitates the area that
327 contains the debris avalanche.

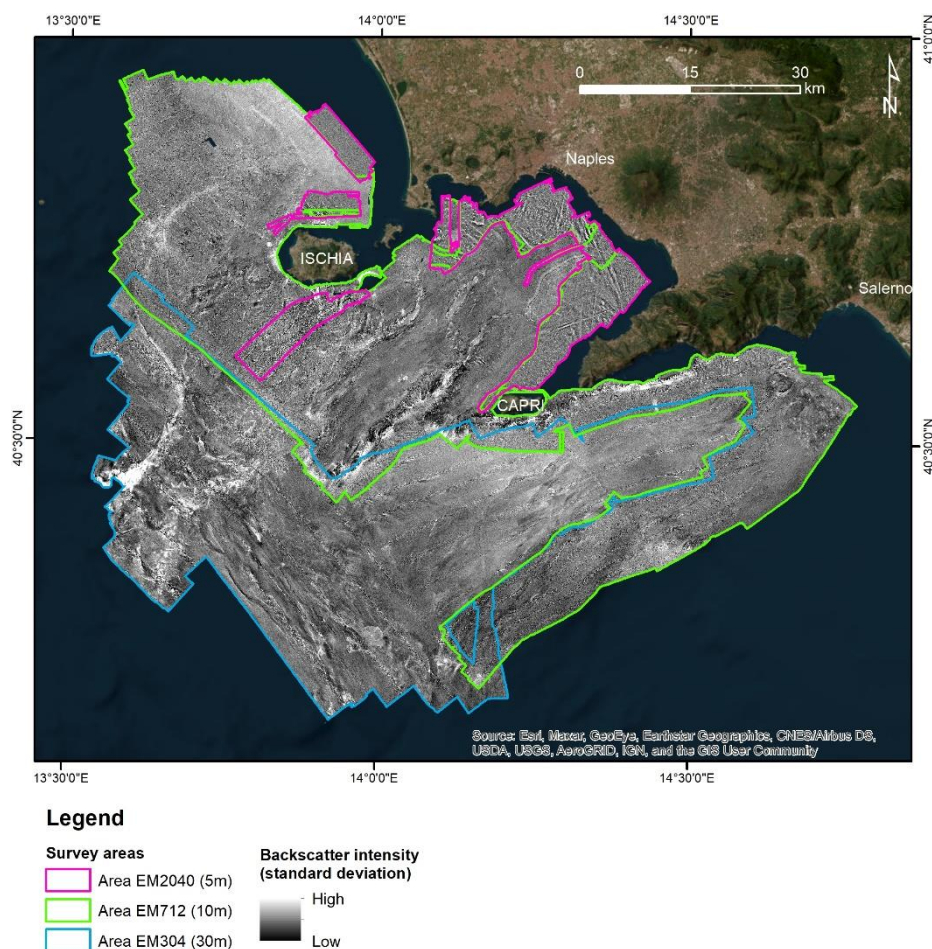
328



329 4.2 The multi-resolution backscatter mosaic

330 The backscatter intensity data acquired during the JammeGaia22 cruise represent the first dataset covering the entire Gulf of
331 Naples, Ischia surroundings, Salerno Valley and Sirene Smt. Three mosaics were exported at different spatial resolutions: 5 m
332 for the dataset acquired using the EM2040 system, 10 m for EM712 and 30 m for EM304 (Figure).

333



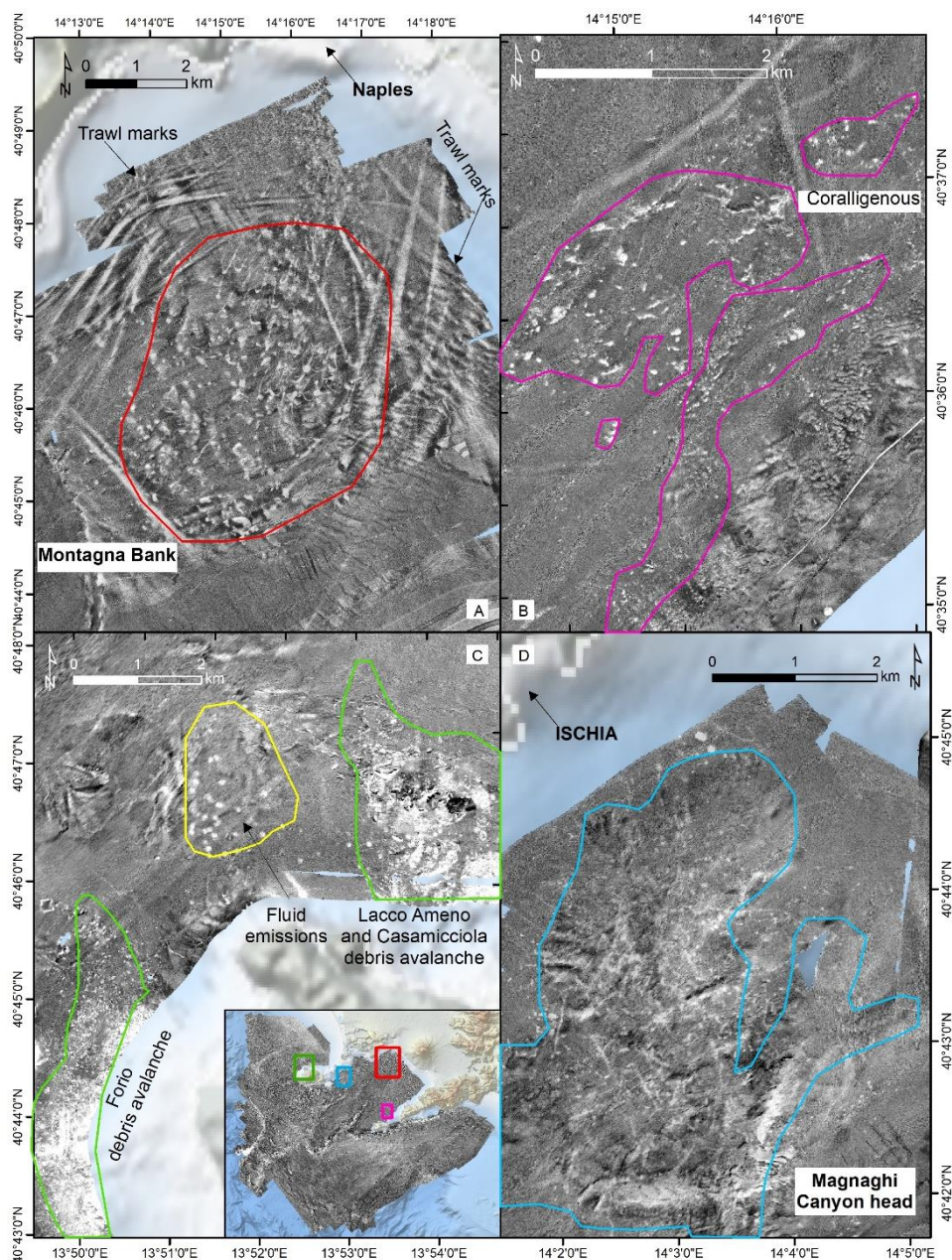
334

335 Figure 8. Backscatter mosaics acquired during the JammeGaia22 cruise with the survey areas covered by the three MBES.

336 Details are shown for four areas: Montagna Bank, Sorrento peninsula, north and west Ischia Island, and Magnaghi canyon
337 head (Figure 8). The backscatter highlighted the hummocky-like morphology of the Montagna Bank and the trawl marks on
338 the seabed around it. The backscatter dataset of the Sorrento peninsula revealed the occurrence of patterns likely associated
339 with coralligenous bioconstructions (the lighter areas) and seagrass meadows along the coast, as previously highlighted in
340 other studies (CARG - Geological CARTography project; EMODnet Seagrass cover (Essential Ocean Variable) in European
341 waters (2023); Russo et al. 2008; Buonocore et al., 2020). Also, the hummocky morphology of the debris avalanches occurring



342 north and west of Ischia Island is enhanced by the seabed reflectivity, together with features of fluid escapes (white spots in
343 Figure 8C) around Ischia Island and in the head of the Magnaghi canyon, due to the hydrothermal activity characterizing the
344 area.
345



346
347 Figure 9. Details of the seabed backscatter in different locations: A) Montagna Bank hummocky morphology and trawl marks (EM2040 –
348 5m); B) Coralligenous bioconstructions west of the Sorrento peninsula (EM712 – 10m); C) debris avalanches north and west of Ischia
349 Island and fluid escape features (EM712 – 10m); D) head of the Magnaghi Canyon characterized by fluid escape features (EM712 – 10m).



350

351 **4.3 MBES data quality**

352 The uncertainty of the bathymetric data was calculated in Qimera v.2.5.4 according to the IHO Standards for Hydrographic
 353 Surveys 2-44 6th Edition, 2022. Total Horizontal Uncertainty (THU) and Total Vertical Uncertainty (TVU) were calculated
 354 considering the standard deviation offsets of the MRU, MBES, sound velocity probe, and positioning system. Parameters used
 355 for the calculation of THU and TVU were taken from the datasheet of the MBES systems and installation report (Table 6).
 356 The uncertainty values of EM2040 vary depending on the sampling frequency and depth changes during the survey. Hence,
 357 the values presented below are the range of uncertainty calculated for 200 kHz and 300 kHz and different pulse lengths that
 358 were used during acquisition.

359

360

Table 6. Parameters used to calculate Total Horizontal Uncertainty and Total Vertical Uncertainty

	EM2040	EM712	EM304
Echosounder			
Pulse Length	2, 3, 6, and 12 ms	2 ms	7.5 ms
Sampling Frequency	200kHz, 300 kHz,	70 kHz	25 kHz
Sound Velocity			
SD Surface sound speed	0.02 m/s	0.02 m/s	0.02 m/s
Beam Width			
Beam Width Along (Tx)	0.4°	0.5°	1.0°
Beam Width Across (Rx)	0.7°	1.0°	1.0°
Offsets (Argo)			
SD Roll Offset	0.04°	0.04°	0.04°
SD Pitch Offset	0.02°	0.02°	0.02°
SD Heading Offset	0.02°	0.02°	0.02°
POS			
SD Horizontal	0.1 m	0.1 m	0.1 m
SD Vertical	0.1 m	0.1 m	0.1 m

361

362 The results show the lowest horizontal uncertainty for data collected using EM2040 (THU = 1.66 to 4.94 m), while those
 363 collected with EM304 present the highest uncertainty (THU = 20.03 m) (Table 7). The lowest vertical uncertainty was obtained
 364 for EM712 (TVU= 1.29 m), whilst the highest for EM2040 (TVU = 4.77 m). Uncertainties of the collected data for all the
 365 systems fell within the limits of the IHO Standards for a specific water depth or Order number.

366

367

368



369

370 Table 7. Mean horizontal and vertical uncertainties of bathymetric data collected using different multibeam systems, and the accepted IHO
371 error limits, which shows that the data collected are within the IHO standards.

372

THU (m)	TVU (m)	IHO S44 6th Order Error Limit	IHO S44 6th Order No.
EM2040	1.66 - 4.94	0.88 - 4.77	2.57
EM712	8.98	1.29	5.28
EM304	20.03	3.67	22.80

373

374

375 The uncertainty values calculated for JammeGaia22 survey data testify that the seafloor map of the Gulf of Naples obtained
376 with the innovative technologies installed on board the R/V Gaia Blu represents a product of high quality. This new dataset
377 will serve as a crucial baseline for future in-depth analysis of the geomorphology of the area, favoring the identification of
378 seabed features at unprecedented resolution.

379 A significant improvement in the resolution of the data appears evident when comparing the morphology of the Ischia debris
380 avalanche from DTM at 20 m horizontal resolution generated from the ancient and modern datasets. The newly acquired
381 dataset shows better coverage and less noise than the 2001 dataset (Figure 9). The blocks of the landslide deposit can be also
382 clearly identified in the new dataset whilst the identification is not obvious for some areas in the 2001 dataset.

383 To test if this increase in the resolution has an impact on geomorphological indices derived from the bathymetry, we calculated
384 the fine-scale BPI from the 20 m-resolution DTMs (2001 and the JammeGaia22 surveys) using the same parameters for both
385 the datasets, reported in Table 5. The results show a much higher noise level for the 2001 DTM with respect to the
386 JammeGaia22 dataset (Figure 10). The noise was higher especially at the overlap among the swaths on the western part of the
387 dataset, and the central beams of the swath in the central part of the data, where most of the landslide blocks occur. Such blocks
388 are better detected and isolated through BPIs in 2022 DTM, rather than in 2001 DTM.

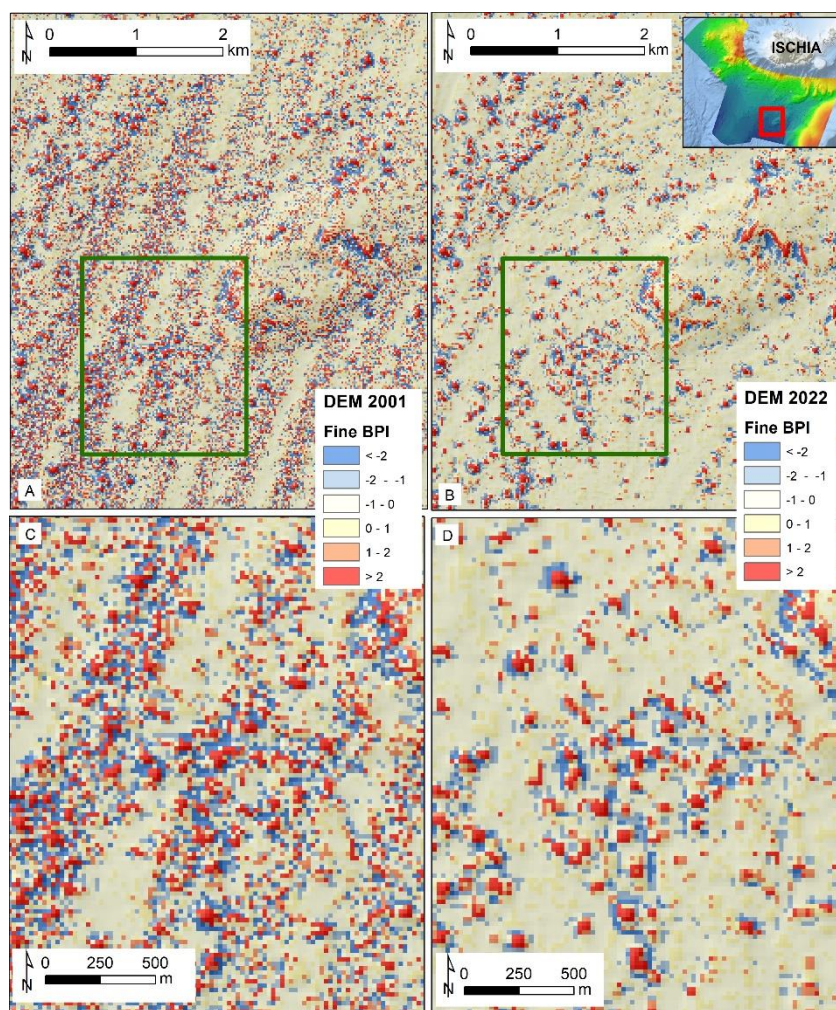
389

390 **4.4 Comparison to previous data**

391 The area for this study was selected not only for its intriguing dynamic, tectonic and volcanic activity, benthic boundary
392 processes and seafloor biodiversity, and widespread human impacts of various origins. An additional reason was offered by
393 the opportunity to compare the newly acquired data with a previous high-standard multibeam study of the area. In fact, this
394 area has been already mapped since the late '90s with state of the art (for that time) instrumentation and presented in extremely
395 accurate and imaginative 3D views (D'Argenio et al., 2004; de Alteriis et al., 2010; Passaro et al., 2014; Sacchi et al., 2014;
396 Budillon et al., 2016; Paoletti et al., 2016; Passaro et al., 2016a, 2016b; Di Martino et al., 2021; Aiello and Sacchi, 2022). The
397 limitation of that original database came from the need to acquire the data in a succession of surveys spanning several years
398 and using instruments with rather variable resolutions. Nevertheless, also thanks to the extreme accuracy of the data processing



399 performed at that time, this 20-year-old database provided an excellent basis for comparison with the newly acquired, more
400 homogenous, database. Of course, the comparison cannot be pushed to the highest resolution offered by the modern
401 instruments on Gaia Blu but, even on lower resolution, the comparison among 20 m grids from the two data sets can be
402 extremely valuable.
403



404
405
406
407
408
409

Figure 10. Fine-scale BPI calculated on the 2001 DTM (A) and JammeGaia22 DTM (B) for the area of the Ischia debris avalanche; noticeably, the 2001 dataset is very noisy. Detail of the blocks accumulation for 2001 DTM (C) and JammeGaia22 DTM (D): despite both datasets have same spatial resolution (20 m), the newly acquired dataset allows to better discriminate and map blocks.



410 **5. Data availability**

411 All datasets, products and web services are managed through the ISMAR Marine Spatial Data Infrastructure – MSDI (Foglini
 412 & Grande 2023) and follow the ISMAR-CNR Data policy (<https://doi.org/10.26383/CNR-ISMAR.2023.6>). Bathymetric
 413 datasets gathered by the MBES in the format GSF (generic sensor format), and bathymetric and backscatter surfaces (GeoTIFF)
 414 are shared in the Marine Geoscience Data System (MGDS) (Table 8).

415 Data are also available as Web Map Services (WMS), that are interoperable with other infrastructures and permit the integration
 416 of the spatial data in other geoportals or directly in a desktop environment (e.g., QGIS, ArcMap). Data are free accessible
 417 thought two main interfaces: the metadata catalogue and the WebGIS.

418 The CNR-ISMAR GeoNetwork metadata catalogue (<https://www.ismar.cnr.it/en/infrastructures/information-resources/geo->
 419 [portals/#2](https://www.ismar.cnr.it/en/infrastructures/information-resources/geo-portals/#2)) allows users to find the JammeGaia22 products (refer to Table 8 for direct links to products), containing information
 420 about access and use policy, link to download the data, how to cite the data, DOI, and links to external repositories (such as
 421 EMODnet and MGDS). The WebGIS (<https://www.ismar.cnr.it/en/infrastructures/information-resources/geo-portals/#1>)
 422 publishes survey areas, multibeam navigation lines, bathymetric surfaces and backscatter mosaics. Users can navigate the map
 423 to the JammeGaia22 survey area, explore the layer list and open the geophysical data and products. By clicking on spatial
 424 objects on the map, users can access the related information, such as the download link.

425 Table 8. Products of the JammeGaia22 oceanographic cruise with relative link.

Product	Typology	Depth range	Spatial resolution	Format	Link CNR-ISMAR Catalog	DOIs
Survey JAMME GAIA 2022	Cruise report	-	-	PDF	http://libeccio.bo.ismar.cnr.it:8080/geonetwark/srv/eng/catalog.search#/metadata/6cd1080c-f41f-4c9d-907b-297d25f554e5	Foglini, et al., 2024a, https://doi.org/10.26383/CNR-ISMAR.2024.4
JG22_SwathLines_EM2040	MBES processed lines	-	-	GSF	http://libeccio.bo.ismar.cnr.it:8080/geonetwark/srv/eng/catalog.search#/metadata/6213658d-ca9a-4e40-af07-e4f7b329203a	Foglini, 2024a http://dx.doi.org/10.60521/331589
JG22_SwathLines_EM712	MBES processed lines	-	-	GSF	http://libeccio.bo.ismar.cnr.it:8080/geonetwark/srv/eng/catalog.search#/metadata/62136	Foglini 2024b



					58d-ca9a-4e40-af07-e4f7b329203a	http://dx.doi.org/10.60521/331587
JG22_SwathLines_EM304	MBES processed lines	-	-	GSF	http://libeccio.bo.ismar.cnr.it:8080/geonetwark/srv/eng/catalog.search#/metadata/6213658d-ca9a-4e40-af07-e4f7b329203a	Foglini 2024c, http://dx.doi.org/10.60521/331584
JG22_50_120_2m	Bathymetric surface	50-120 m	2 m	ASCII GeoTIFF ESRI_grid	http://libeccio.bo.ismar.cnr.it:8080/geonetwark/srv/eng/catalog.search#/metadata/927334e6-021a-4eed-a0a6-f209df3b17ad	Foglini et al. 2024b, http://dx.doi.org/10.60521/331667
JG22_100_200_5m	Bathymetric surface	100 -200 m	5 m	ASCII GeoTIF ESRI_grid	http://libeccio.bo.ismar.cnr.it:8080/geonetwark/srv/eng/catalog.search#/metadata/5e384b50-ea4d-4e68-b023-d5b64ebd5ed8	
JG22_180_500_10m	Bathymetric surface	180-500 m	10 m	ASCII GeoTIFF ESRI_grid	http://libeccio.bo.ismar.cnr.it:8080/geonetwark/srv/eng/catalog.search#/metadata/e956cee4-ba1c-41b7-932b-4031932c9a9d	
JG22_480_700_15m	Bathymetric surface	480-700 m	15 m	ASCII GeoTIFF ESRI_grid	http://libeccio.bo.ismar.cnr.it:8080/geonetwark/srv/eng/catalog.search#/metadata/5124f1d9-982c-4996-8333-298eb62e5c73	
JG22_680_1000_20m	Bathymetric surface	680-1000 m	20 m	ASCII GeoTIFF ESRI_grid	http://libeccio.bo.ismar.cnr.it:8080/geonetwark/srv/eng/catalog.search#/metadata/21481	



					1a5-1700-413f-9b3f-95d2ddd29996	
JG22_980_1300_30m	Bathymetric surface	980-1300 m	30 m	ASCII GeoTIFF ESRI_grid	http://libeccio.bo.ismar.cnr.it:8080/geonetwark/srv/eng/catalog.search#/metadata/a43cf1d4-abc6-43e4-9f66-fac08827c5dd	
JG22_1280_2120_40m	Bathymetric surface	1280-2120 m	40 m	ASCII GeoTIFF ESRI_grid	http://libeccio.bo.ismar.cnr.it:8080/geonetwark/srv/eng/catalog.search#/metadata/96388cc5-2c58-4ba3-9816-7231c69d96e8	
JG22_2040_5m	Backscatter mosaic from EM2040	-	5 m	ASCII GeoTIFF ESRI_grid	http://libeccio.bo.ismar.cnr.it:8080/geonetwark/srv/eng/catalog.search#/metadata/6ec52054-ac6c-46e6-966b-8a88d1cf4351	
JG22_712_10m	Backscatter mosaic from EM712	-	10 m	ASCII GeoTIFF ESRI_grid	http://libeccio.bo.ismar.cnr.it:8080/geonetwark/srv/eng/catalog.search#/metadata/d4c1635f-69f2-4ebc-9174-d2a9d60a1e58	Foglini et al. 2024c, http://dx.doi.org/10.60521/331668
JG22_304_30m	Backscatter mosaic from EM304	-	30 m	ASCII GeoTIFF ESRI_grid	http://libeccio.bo.ismar.cnr.it:8080/geonetwark/srv/eng/catalog.search#/metadata/94f61db5-c186-48a6-b82b-7d9685c2a541	

426

427 6. Conclusions

428 The JammeGaia22 cruise led to the creation of a multi-resolution DTM and backscatter mosaic for the Gulf of Naples, by
 429 using three different state-of-the-art MBESs. The dataset has been obtained through a reproducible processing workflow and



430 corresponds to a major upgrade of a pre-existing bathymetry of the area. The vertical and positioning uncertainties of the
431 bathymetric data fall within the IHO standards and satisfy Order 1b for EM2040 and Order 2 for EM712 and EM304.
432 The newly acquired multi beam maps reveal submerged morphologies at a scale and resolution never achieved before for the
433 study area, allowing for a wide range of local and regional studies, spanning from geological and geomorphological research
434 to marine habitat mapping and sea-floor monitoring. Furthermore, these high-resolution bathymetry and backscatter datasets
435 can be useful for Maritime spatial Planning and for designing innovative conservation strategies.
436 The new data base is released to the community as a benchmark reference against which future sea-floor changes can be
437 quantified and ascribed to either the activity of subaqueous volcanic apparatuses, in particular in the vicinity of the Flegraean
438 Field, the flux of density flows along major conduits like Cuma Channel, and Magnaghi and Dohrn Canyons, slope instability
439 leading to mass-transport deposits or sand splays at the mouth of slope gullies. Large scale bedforms are particularly developed
440 in regions flow rearrangement like in a bend of Cuma Channel, west of Ischia Island, or in the area of possible cyclic steps, on
441 the slope south of Ischia. Backscatter data help recognizing areas of potential occurrence of white coral colonies, a key element
442 of the Mediterranean biodiversity richness. Finally, both bathymetric and backscatter data help define the areas most impacted
443 by fish trawling, smoothing and remoulding the seafloor, illegal dumping and diffused littering.

444 **7. Author contribution**

445 FF: Supervisor, data collection and processing, conceptualisation, and writing; MR: Supervisor, data collection,
446 conceptualisation; RT: Supervisor, data collection and processing; GC, DG: data collection, data processing, first draft writing;
447 VG, MP: data management, data processing, first draft writing; LP, CP, FB, FM, MC, MS, ML, PM data collection and review;
448 GD, SI, ANT, AP, AM, AR data collection and processing; FT: Supervisor and review.

449 **8. Competing interests**

450 The contact author has declared that none of the authors has any competing interests.

451 **9. Acknowledgements**

452 We thank captain, crew, and scientific staff of R/V Gaia Blu for their skilful and efficient cooperation during operations at sea.
453 This is ISMAR-Bologna scientific contribution no. 2088.



454 References

- 455 Aiello, G., Iorio, M., Molisso, F., and Sacchi, M.: Integrated Morpho-Bathymetric, Seismic-Stratigraphic, and
456 Sedimentological Data on the Dohrn Canyon (Naples Bay, Southern Tyrrhenian Sea): Relationships with
457 Volcanism and Tectonics, *Geosciences*, 10, 319, <https://doi.org/10.3390/geosciences10080319>, 2020.
- 458 Aiello, G., Sacchi, M.: New morpho-bathymetric data on marine hazard in the offshore of Gulf of Naples (Southern
459 Italy). *Natural Hazards* 111(3), 2881-2908, 2022.
- 460 Albert, P. G., Giaccio, B., Isaia, R., Costa, A., Niespolo, E. M., Nomade, S., Pereira, A., Renne, P. R., Hinchliffe,
461 A., Mark, D. F., Brown, R. J., and Smith, V. C.: Evidence for a large-magnitude eruption from Campi Flegrei
462 caldera (Italy) at 29 ka, *Geology*, 47, 595–599, <https://doi.org/10.1130/G45805.1>, 2019.
- 463 Amato, V., Aucelli, P. P. C., Cinque, A., D’Argenio, B., Donato, V. D., Pappone, G., Petrosino, P., Roszkopf, C.
464 M., and Ermolli, E. R.: Holocene palaeo-geographical evolution of the Sele river coastal plain (Southern Italy):
465 new morpho-sedimentary data from the Paestum area, *Alpine and Mediterranean Quaternary*, 24, 5–7, 2011.
- 466 Angiolillo, M., Bo, M., Toma, M., Giusti, M., Salvati, E., Giova, A., Lagudi, A., Rossi, L., Collina, M., Bruno, F.,
467 Canese, S., and Tunesi, L.: A baseline for the monitoring of Mediterranean upper bathyal biogenic reefs within the
468 marine strategy framework directive objectives, *Deep Sea Research Part I: Oceanographic Research Papers*, 194,
469 103963, <https://doi.org/10.1016/j.dsr.2023.103963>, 2023.
- 470 Appolloni, L., Sandulli, R., Vetrano, G., and Russo, G. F.: A new approach to assess marine opportunity costs and
471 monetary values-in-use for spatial planning and conservation; the case study of Gulf of Naples, Mediterranean Sea,
472 Italy, *Ocean & Coastal Management*, 152, 135–144, <https://doi.org/10.1016/j.ocecoaman.2017.11.023>, 2018.
- 473 Appolloni, L., Zeppilli, D., Donnarumma, L., Baldrighi, E., Chianese, E., Russo, G., and Sandulli, R.: Seawater
474 Acidification Affects Beta-Diversity of Benthic Communities at a Shallow Hydrothermal Vent in a Mediterranean
475 Marine Protected Area (Underwater Archaeological Park of Baia, Naples, Italy), *Diversity*, 12, 464,
476 <https://doi.org/10.3390/d12120464>, 2020.
- 477 Basterretxea, G., Font-Muñoz, J. S., Salgado-Hernanz, P. M., Arrieta, J., and Hernández-Carrasco, I.: Patterns of
478 chlorophyll interannual variability in Mediterranean biogeographical regions, *Remote Sensing of Environment*,
479 215, 7–17, <https://doi.org/10.1016/j.rse.2018.05.027>, 2018.
- 480 Bavestrello, G., Bo, M., Canese, S., Sandulli, R., and Cattaneo-Vietti, R.: The red coral populations of the gulfs of
481 Naples and Salerno: human impact and deep mass mortalities, *Italian Journal of Zoology*, 81, 552–563,
482 <https://doi.org/10.1080/11250003.2014.950349>, 2014.
- 483 Beaudoin, J., Renoud, W., Mohammadloo, T. H., & Snellen, M. Automated correction of refraction residuals. In
484 HYDRO18 conference, 2018.
- 485 Bellucci, F., Milia, A., Rolandi, G., and Torrente, M. M.: Chapter 8 Structural control on the Upper Pleistocene
486 ignimbrite eruptions in the Neapolitan area (Italy): volcano tectonic faults versus caldera faults, in: *Developments*
487 *in Volcanology*, vol. 9, edited by: De Vivo, B., Elsevier, 163–180, [https://doi.org/10.1016/S1871-644X\(06\)80022-](https://doi.org/10.1016/S1871-644X(06)80022-7)
488 [7](https://doi.org/10.1016/S1871-644X(06)80022-7), 2006.



- 489 Bianchi, C. N. and Morri, C.: Marine Biodiversity of the Mediterranean Sea: Situation, Problems and Prospects for
490 Future Research, *Marine Pollution Bulletin*, 40, 367–376, [https://doi.org/10.1016/S0025-326X\(00\)00027-8](https://doi.org/10.1016/S0025-326X(00)00027-8), 2000.
- 491 Budillon, F., Violante, C., De Lauro M. I fondali delle Isole Flegree, morfologia e geologia. in: *Ambiente marino*
492 *costiero e territorio delle isole flegree (Ischia Procida e Vivara – Golfo di Napoli)*. Risultati di uno studio
493 multidisciplinare, edited by: Gambi, M. C., De Lauro, M., Jannuzzi, F., *Mem. Acc. Sci. Fis. E Matem.*, Napoli 5,
494 45-66, 2003.
- 495 Budillon, F., Cesarano, M., Conforti, A., Pappone, G., Di Martino, G., Pelosi, N.: Recurrent superficial sediment
496 failure and deep gravitational deformation in a Pleistocene slope marine succession: The *Poseidonia* slide (Salerno
497 Bay, Tyrrhenian Sea), *Submarine Mass Movements and Their Consequences*, 6th International Symposium, 273-
498 283, 2016.
- 499 Budillon F., Firetto Carlino M., Innangi S., Passaro S., Tonielli R., Trincardi F., Sprovieri M. (2022). The
500 Anthropogenic Footprint of Physical Harm on the Seabed of Augusta Bay (Western Ionian Sea). *Journal of Marine*
501 *Science and Engineering* 10 (11), 1737. Buonocore, E., Appolloni, L., Russo, G. F., and Franzese, P. P.: Assessing
502 natural capital value in marine ecosystems through an environmental accounting model: A case study in Southern
503 Italy, *Ecological Modelling*, 419, 108958, <https://doi.org/10.1016/j.ecolmodel.2020.108958>, 2020.
- 504 Canals, M., Pham, C. K., Bergmann, M., Gutow, L., Hanke, G., Sebille, E. van, Angiolillo, M., Buhl-Mortensen,
505 L., Cau, A., Ioakeimidis, C., Kammann, U., Lundsten, L., Papatheodorou, G., Purser, A., Sanchez-Vidal, A.,
506 Schulz, M., Vinci, M., Chiba, S., Galgani, F., Langenkämper, D., Möller, T., Nattkemper, T. W., Ruiz, M.,
507 Suikkanen, S., Woodall, L., Fakiris, E., Jack, M. E. M., and Giorgetti, A.: The quest for seafloor macrolitter: a
508 critical review of background knowledge, current methods and future prospects, *Environ. Res. Lett.*, 16, 023001,
509 <https://doi.org/10.1088/1748-9326/abc6d4>, 2021.
- 510 CARG (Geological CARTography) project: [https://www.isprambiente.gov.it/en/projects/soil-and-territory/carg-](https://www.isprambiente.gov.it/en/projects/soil-and-territory/carg-project-geologic-and-geothematic-cartography)
511 [project-geologic-and-geothematic-cartography](https://www.isprambiente.gov.it/en/projects/soil-and-territory/carg-project-geologic-and-geothematic-cartography) (last access: 28 February 2024)
- 512 Chiocci, F. L. and De Alteriis, G.: The Ischia debris avalanche: first clear submarine evidence in the Mediterranean
513 of a volcanic island prehistorical collapse, *Terra Nova*, 18, 202–209, [https://doi.org/10.1111/j.1365-](https://doi.org/10.1111/j.1365-3121.2006.00680.x)
514 [3121.2006.00680.x](https://doi.org/10.1111/j.1365-3121.2006.00680.x), 2006.
- 515 Coll, M., Piroddi, C., Albouy, C., Ben Rais Lasram, F., Cheung, W. W. L., Christensen, V., Karpouzi, V. S.,
516 Guilhaumon, F., Mouillot, D., Paleczny, M., Palomares, M. L., Steenbeek, J., Trujillo, P., Watson, R., and Pauly,
517 D.: The Mediterranean Sea under siege: spatial overlap between marine biodiversity, cumulative threats and marine
518 reserves, *Global Ecology and Biogeography*, 21, 465–480, <https://doi.org/10.1111/j.1466-8238.2011.00697.x>,
519 2012.
- 520 D’Argenio, B., Angelino, A., Aiello, G., de Alteriis, G., Milia, A., Sacchi, M., Tonielli, R., Budillon, F., Chiocci,
521 F. L., Conforti, A., Lauro, M., Di Martino, G., D’Isanto, C., Esposito, E., Ferraro, L., Innangi, S., Insinga, D. D.,
522 Iorio, Marsella, E., Molisso, F., Morra, V. B., Passaro, S., Pelosi, N., Pordo, S., Raspini, A., Ruggeri, S.,
523 Sarnacchiaro, G., Terranova, C., Vilardo, G., and Violante, C.: Digital elevation model of the Naples Bay and
524 adjacent areas (Eastern Tyrrhenian Sea), in: *Mapping Geology in Italy, Atlante di Cartografia Geologica*, vol.
525 *Convegno Internazionale Firenze*, edited by: Pasquare, E. and Venturini, G., Firenze, Italy, 21–28, 2004.



- 526 de Alteriis, G., Insinga, D. D., Morabito, S., Morra, V., Chiocci, F. L., Terrasi, F., Lubritto, C., Di Benedetto, C.,
527 and Pazzanese, M.: Age of submarine debris avalanches and tephrostratigraphy offshore Ischia Island, Tyrrhenian
528 Sea, Italy, *Marine Geology*, 278, 1–18, <https://doi.org/10.1016/j.margeo.2010.08.004>, 2010.
- 529 Deino, A. L., Orsi, G., de Vita, S., and Piochi, M.: The age of the Neapolitan Yellow Tuff caldera-forming eruption
530 (Campi Flegrei caldera – Italy) assessed by $^{40}\text{Ar}/^{39}\text{Ar}$ dating method, *Journal of Volcanology and Geothermal*
531 *Research*, 133, 157–170, [https://doi.org/10.1016/S0377-0273\(03\)00396-2](https://doi.org/10.1016/S0377-0273(03)00396-2), 2004.
- 532 Díaz, S., Settele, J., Brondízio, E. S., Ngo, H. T., Agard, J., Arneeth, A., Balvanera, P., Brauman, K. A., Butchart,
533 S. H. M., Chan, K. M. A., Garibaldi, L. A., Ichii, K., Liu, J., Subramanian, S. M., Midgley, G. F., Miloslavich, P.,
534 Molnár, Z., Obura, D., Pfaff, A., Polasky, S., Purvis, A., Razzaque, J., Reyers, B., Chowdhury, R. R., Shin, Y.-J.,
535 Visseren-Hamakers, I., Willis, K. J., and Zayas, C. N.: Pervasive human-driven decline of life on Earth points to
536 the need for transformative change, *Science*, 366, eaax3100, <https://doi.org/10.1126/science.aax3100>, 2019.
- 537 Di Martino, G., Innangi, S., Sacchi, M., Tonielli, R.: Seafloor morphology changes in the inner-shelf area of the
538 Pozzuoli Bay, Eastern Tyrrhenian Sea, *Marine Geophysical Research*, 42(2),13, 2021.
- 539 Dolan, M. F. J.: Calculation of slope angle from bathymetry data using GIS - effects of computation algorithm,
540 data resolution and analysis scale, 2012.
- 541 Donnarumma, L., Appolloni, L., Chianese, E., Bruno, R., Baldrighi, E., Guglielmo, R., Russo, G. F., Zeppilli, D.,
542 and Sandulli, R.: Environmental and Benthic Community Patterns of the Shallow Hydrothermal Area of Secca
543 Delle Fumose (Baia, Naples, Italy), *Front. Mar. Sci.*, 6, 685, <https://doi.org/10.3389/fmars.2019.00685>, 2019.
- 544 EMODnet Seagrass cover (Essential Ocean Variable) in European waters (2023):
545 [https://emodnet.ec.europa.eu/geonetwork/emodnet/eng/catalog.search#/metadata/39746d9c-4220-425c-bc26-](https://emodnet.ec.europa.eu/geonetwork/emodnet/eng/catalog.search#/metadata/39746d9c-4220-425c-bc26-7cb3056c36a5)
546 [7cb3056c36a5](https://emodnet.ec.europa.eu/geonetwork/emodnet/eng/catalog.search#/metadata/39746d9c-4220-425c-bc26-7cb3056c36a5) (last access: 28 February 2024).
- 547 Foglini, F. Processed EM2040 Acoustic Backscatter and Swath Bathymetry data from R/V Gaia Blu cruise Jamme
548 Gaia22 (2022). MGDS. 2024a, doi:10.60521/331589
- 549 Foglini, F. Processed EM712 Acoustic Backscatter and Swath Bathymetry data from R/V Gaia Blu cruise Jamme
550 Gaia22 (2022). MGDS. 2024b, doi:[10.60521/331587](https://doi.org/10.60521/331587)
- 551 Foglini, F. Processed EM304 Acoustic Backscatter and Swath Bathymetry data from R/V Gaia Blu cruise Jamme
552 Gaia22 (2022). MGDS. 2024c, doi:[10.60521/331584](https://doi.org/10.60521/331584)
- 553 Foglini, F. and Grande, V.: A Marine Spatial Data Infrastructure to manage multidisciplinary, inhomogeneous and
554 fragmented geodata in a FAIR perspective ... the Adriatic Sea experience, *Oceanologia*, 65, 260–277,
555 <https://doi.org/10.1016/j.oceano.2022.11.002>, 2023.
- 556 Foglini, F., Tonielli, R., and Rovere M. Cruise report Survey JAMME GAIA 2022. CNR-ISMAR, 2024a,
557 <https://doi.org/10.26383/CNR-ISMAR.2024.4>
- 558 Foglini, F.; Tonielli, R. and M. Rovere. Multi-Resolution bathymetry grids of the Naples and Pozzuoli Gulf and
559 the Amalfi Coastal Area collected during cruise Jamme_Gaia22, 2022. MGDS. 2024b, doi:[10.60521/331667](https://doi.org/10.60521/331667)



- 560 Foglini, F.; Tonielli, R. and M. Rovere. Multi-Resolution backscatter grids of the Naples and Pozzuoli Gulf and
561 the Amalfi Coastal Area collected during cruise Jamme_Gaia22, 2022. MGDS, 2024c,
562 doi:10.60521/331668Giaccio, B., Isaia, R., Fedele, F. G., Di Canzio, E., Hoffecker, J., Ronchitelli, A., Sinitsyn, A.
563 A., Anikovitch, M., Lisitsyn, S. N., and Popov, V. V.: The Campanian Ignimbrite and Codola tephra layers: Two
564 temporal/stratigraphic markers for the Early Upper Palaeolithic in southern Italy and eastern Europe, *Journal of*
565 *Volcanology and Geothermal Research*, 177, 208–226, <https://doi.org/10.1016/j.jvolgeores.2007.10.007>, 2008.
- 566 Giaccio B., Hajdas I., Isaia R., Deino A., Nomade S. High-precision ^{14}C and $^{40}\text{Ar}/^{39}\text{Ar}$ dating of the Campanian
567 Ignimbrite (Y-5) reconciles the time-scales of climatic-cultural processes at 40 ka. *Sci. Rep.* 7, 45940; doi:
568 10.1038/srep45940, 2017.Iampietro, P. and Kvitek, R.: Iampietro, P., and R. Kvitek. 2002. Quantitative seafloor
569 habitat classification using GIS terrain analysis: Effects of data density, resolution, and scale. In *Proceedings of the*
570 *22nd Annual ESRI User Conference*. San Diego, CA July 8–12, in: *Proceedings of the 22nd Annual ESRI User*
571 *Conference*, 22nd Annual ESRI User Conference, San Diego, CA, 2002.
- 572 Isaia, R., Vitale, S., Marturano, A., Aiello, G., Barra, D., Ciarcia, S., Iannuzzi, E., and Tramparulo, F. D.: High-
573 resolution geological investigations to reconstruct the long-term ground movements in the last 15 kyr at Campi
574 Flegrei caldera (southern Italy), *Journal of Volcanology and Geothermal Research*, 385, 143–158,
575 <https://doi.org/10.1016/j.jvolgeores.2019.07.012>, 2019.
- 576 Kastens, K., Mascle, J., Auroux, C., Bonatti, E., Broglia, C., Channell, J., Curzi, P., Emeis, K.-C., Glaçon, G.,
577 Hasegawa, S., Hieke, W., Mascle, G., McCoy, F., McKenzie, J., Mendelson, J., Müller, C., Réhault, J.-P.,
578 Robertson, A., Sartori, R., Sprovieri, R., and Torii, M.: ODP Leg 107 in the Tyrrhenian Sea: Insights into passive
579 margin and back-arc basin evolution, *GSA Bulletin*, 100, 1140–1156, [https://doi.org/10.1130/0016-7606\(1988\)100<1140:OLITTS>2.3.CO;2](https://doi.org/10.1130/0016-7606(1988)100<1140:OLITTS>2.3.CO;2), 1988.
- 581 Kostic, S.: Modeling of submarine cyclic steps: controls on their formation, migration, and architecture. *Geosphere*,
582 7(2), 294-304, 2011.
- 583 Le Bas, T. P. RSOBIA: A new OBIA Toolbar and Toolbox in ArcMap 10.x for Segmentation and Classification,
584 in: *Proceedings of GEOBIA 2016 : Solutions and synergies*, 14-16 September 2016, Enschede, Netherlands, 6th
585 *International Conference on Geographic Object-Based Image Analysis, GEOBIA 2016: Solutions & Synergies*,
586 <https://doi.org/10.3990/2.448>, 2016.
- 587 Loreto, M. F., Zitellini, N., Ranero, C. R., Palmiotto, C., and Prada, M.: Extensional tectonics during the Tyrrhenian
588 back-arc basin formation and a new morpho-tectonic map, *Basin Research*, 33, 138–158,
589 <https://doi.org/10.1111/bre.12458>, 2021.
- 590 Lucchi, F. R., Colella, A., Gabbianelli, G., Rossi, S., & Normark, W. R.: The Crati submarine fan, Ionian sea. *Geo-*
591 *marine letters*, 3, 71-77, 1983.
- 592 Lundblad, E. R., Wright, D. J., Miller, J., Larkin, E. M., Rinehart, R., Naar, D. F., Donahue, B. T., Anderson, S.
593 M., and Battista, T.: A Benthic Terrain Classification Scheme for American Samoa, *Marine Geodesy*, 29, 89–111,
594 <https://doi.org/10.1080/01490410600738021>, 2006.



- 595 Lymer, G., Lofi, J., Gaullier, V., Maillard, A., Thinon, I., Sage, F., Chanier, F., and Vendeville, B. C.: The Western
596 Tyrrhenian Sea revisited: New evidence for a rifted basin during the Messinian Salinity Crisis, *Marine Geology*,
597 398, 1–21, <https://doi.org/10.1016/j.margeo.2017.12.009>, 2018.
- 598 Madricardo, F., Fogliini, F., Campiani, E., Grande, V., Catenacci, E., Petrizzo, A., Kruss, A., Toso, C., and
599 Trincardi, F.: Assessing the human footprint on the sea-floor of coastal systems: the case of the Venice Lagoon,
600 Italy, *Sci Rep*, 9, 6615, <https://doi.org/10.1038/s41598-019-43027-7>, 2019.
- 601 Marine Geoscience Data System – MGDS: <https://www.marine-geo.org/> (last access: 28 February 2024).
- 602 Mattei, G., Rizzo, A., Anfuso, G., Aucelli, P. P. C., and Gracia, F. J.: A tool for evaluating the archaeological
603 heritage vulnerability to coastal processes: The case study of Naples Gulf (southern Italy), *Ocean & Coastal*
604 *Management*, 179, 104876, <https://doi.org/10.1016/j.ocecoaman.2019.104876>, 2019.
- 605 Mayer, L., Jakobsson, M., Allen, G., Dorschel, B., Falconer, R., Ferrini, V., Lamarche, G., Snaith, H., and
606 Weatherall, P.: The Nippon Foundation—GEBCO Seabed 2030 Project: The Quest to See the World’s Oceans
607 Completely Mapped by 2030, *Geosciences*, 8, 63, <https://doi.org/10.3390/geosciences8020063>, 2018.
- 608 Milia, A.: Aggrading and prograding infill of a peri-Tyrrhenian Basin (Naples Bay, Italy), *Geo-Marine Letters*, 19,
609 237–244, <https://doi.org/10.1007/s003670050114>, 1999.
- 610 Milia, A.: The Dohrn canyon: a response to the eustatic fall and tectonic uplift of the outer shelf along the eastern
611 Tyrrhenian Sea margin, Italy, *Geo-Marine Letters*, 20, 101–108, <https://doi.org/10.1007/s003670000044>, 2000.
- 612 Milia, A., Torrente, M. M., Russo, M., and Zuppetta, A.: Tectonics and crustal structure of the Campania
613 continental margin: relationships with volcanism, *Mineralogy and Petrology*, 79, 33–47,
614 <https://doi.org/10.1007/s00710-003-0005-5>, 2003.
- 615 Miramontes, E., Déverchère, J., Pellegrini, C., & Chiarella, D.: Mediterranean Sea evolution and present-day
616 physiography. In *Oceanography of the Mediterranean Sea* (pp. 13-39). Elsevier, 2023.
- 617 Mohammadloo, T. H., Snellen, M., Renoud, W., Beaudoin, J., and Simons, D. G.: Correcting Multibeam
618 Echosounder Bathymetric Measurements for Errors Induced by Inaccurate Water Column Sound Speeds, *IEEE*
619 *Access*, 7, 122052–122068, <https://doi.org/10.1109/ACCESS.2019.2936170>, 2019.
- 620 Moussat, E., Rehault, J.-P., Fabbri, A., and Mascle, G.: Evolution géologique de la Mer Tyrrhénienne, *C. r. Acad.*
621 *sci., Sér. 2, Méc. phys. chim. sci. univers sci. terre*, 301, 491–496, 1985.
- 622 Myers, N., Mittermeier, R. A., Mittermeier, C. G., da Fonseca, G. A. B., and Kent, J.: Biodiversity hotspots for
623 conservation priorities, *Nature*, 403, 853–858, <https://doi.org/10.1038/35002501>, 2000.
- 624 Orsi, G., D’Antonio, M., Vita, S. de, and Gallo, G.: The Neapolitan Yellow Tuff, a large-magnitude trachytic
625 phreatoplinian eruption: eruptive dynamics, magma withdrawal and caldera collapse, *Journal of Volcanology and*
626 *Geothermal Research*, 53, 275–287, [https://doi.org/10.1016/0377-0273\(92\)90086-S](https://doi.org/10.1016/0377-0273(92)90086-S), 1992.
- 627 Passaro, S., Genovese, S., Sacchi, M., Barra, M., Rumolo, P., Tamburrino, S., Mazzola, S., Basilone, G., Placenti,
628 F., Aronica, S., and Bonanno, A.: First hydroacoustic evidence of marine, active fluid vents in the Naples Bay



- 629 continental shelf (Southern Italy), *Journal of Volcanology and Geothermal Research*, 285, 29–35,
630 <https://doi.org/10.1016/j.jvolgeores.2014.08.001>, 2014.
- 631 Passaro, S., Tamburrino, S., Vallefucio, M., Tassi, F., Vaselli, O., Giannini, L., Chiodini, G., Caliro, S., Sacchi,
632 M., Luca Rizzo, A., et al. Seafloor doming driven by degassing processes unveils sprouting volcanism in coastal
633 areas. *Sci. Rep.*, 6, 22448, 2016.
- 634 Passaro, S., Sacchi, M., Tamburrino, S., and Ventura, G.: Fluid Vents, Flank Instability, and Seafloor Processes
635 along the Submarine Slopes of the Somma-Vesuvius Volcano, Eastern Tyrrhenian Margin, *Geosciences*, 8, 60,
636 <https://doi.org/10.3390/geosciences8020060>, 2018.
- 637 Pellegrini, C., Saliu, F., Bosman, A., Sammartino, I., Raguso, C., Mercorella, A., & Rovere, M.: Hotspots of
638 microplastic accumulation at the land-sea transition and their spatial heterogeneity: The Po River prodelta (Adriatic
639 Sea). *Science of The Total Environment*, 895, 164908, <https://doi.org/10.1016/j.scitotenv.2023.164908>, 2023.
- 640 Puig, P., Canals, M., Company, J. B., Martín, J., Amblas, D., Lastras, G., Palanques, A., and Calafat, A. M.:
641 Ploughing the deep sea floor, *Nature*, 489, 286–289, <https://doi.org/10.1038/nature11410>, 2012.
- 642 R Core Team: *R: A Language and Environment for Statistical Computing*, Vienna, Austria, 2019.
- 643 Romano, P., Santo, A., Voltaggio, M. L'evoluzione geomorfologia della Pianura del fiume Volturno (Campania)
644 durante il tardo Quaternario (Pleistocene medio-superiore/Olocene). *Il Quaternario* 7(1): 41–56, 1984.
- 645 Ruberti, D., Buffardi, C., Sacchi, M., and Vigliotti, M.: The late Pleistocene-Holocene changing morphology of
646 the Volturno delta and coast (northern Campania, Italy): Geological architecture and human influence, *Quaternary*
647 *International*, 625, 14–28, <https://doi.org/10.1016/j.quaint.2022.03.023>, 2022.
- 648 Russo, G., Donato, R., and Di Stefano, F.: Gli habitat sottomarini delle coste della Campania, *Biologi Italiani*, 6,
649 2008.
- 650 Sacchi, M., Insinga, D., Milia, A., Molisso, F., Raspini, A., Torrente, M. M., and Conforti, A.: Stratigraphic
651 signature of the Vesuvius 79 AD event off the Sarno prodelta system, Naples Bay, *Marine Geology*, 222–223, 443–
652 469, <https://doi.org/10.1016/j.margeo.2005.06.014>, 2005.
- 653 Sacchi, M., Molisso, F., Violante, C., Esposito, E., Insinga, D. D., Lubritto, C., Porfido, S., and Toth, T.: Insight
654 into flood dominated, mixed slioclastic-volcanoclastic fan deltas: very high-resolution seismic examples off the
655 Amalfi cliffed coast, Eastern Tyrrhenian Sea, in: *Geohazard in rocky coastal areas*, edited by: Violante, C.,
656 Geological Society, London, UK, 32–71, 2009.
- 657 Sacchi, M., Pepe, F., Corradino, M., Insinga, D.D., Molisso, F., Lubritto, C.: The Neapolitan Yellow Tuff caldera
658 offshore the Campi Flegrei: Stratal architecture and kinematic reconstruction during the last 15ky, *Marine Geology*,
659 354, 15-33, 2014
- 660 Sacchi, M., Caccavale, M., Corradino, M., Esposito, G., Ferranti, L., Hámori, Z., † F., Insinga, D., Marino, C.,
661 Matano, F., Molisso, F., Natale, J., Passaro, S., Pepe, F., and Toth, T.: The use and beauty of ultra-high-resolution
662 seismic reflection imaging in Late Quaternary marine volcanoclastic settings, Napoli Bay, Italy, *Földtani Közlöny*,
663 149, 371, <https://doi.org/10.23928/foldt.kozl.2019.149.4.371>, 2019.



- 664 Sievers, J., Milbradt, P., Ihde, R., Valerius, J., Hagen, R., and Plüß, A.: An integrated marine data collection for
665 the German Bight – Part 1: Subaqueous geomorphology and surface sedimentology (1996–2016), *Earth System*
666 *Science Data*, 13, 4053–4065, <https://doi.org/10.5194/essd-13-4053-2021>, 2021.
- 667 Slotman, A., & Cartigny, M. J.: Cyclic steps: review and aggradation-based classification. *Earth-Science Reviews*,
668 201, 102949, 2020.
- 669 Somma, R., Iuliano, S., Matano, F., Molisso, F., Passaro, S., Sacchi, M., Troise, C., De Natale, G.: High - resolution
670 morpho-bathymetry of Pozzuoli Bay, southern Italy, *Journal of Maps*, 12(2), 222-230, 2016.
- 671 Stall, S., Yarmey, L., Cutcher-Gershenfeld, J., Hanson, B., Lehnert, K., Nosek, B., Parsons, M., Robinson, E., and
672 Wyborn, L.: Make scientific data FAIR, *Nature*, 570, 27–29, <https://doi.org/10.1038/d41586-019-01720-7>, 2019.
- 673 Steinmann, L., Spiess, V., Sacchi, M.: The Campi Flegrei caldera (Italy): Formation and evolution in interplay with
674 sea-level variations since the Campanian Ignimbrite eruption at 39 ka. *Journal of Volcanology and Geothermal*
675 *Research* 327, 361-374, 2016.
- 676 Tanhua, T., Hainbucher, D., Cardin, V., Álvarez, M., Civitarese, G., McNichol, A. P., and Key, R. M.: Repeat
677 hydrography in the Mediterranean Sea, data from the *Meteor* cruise 84/3 in 2011, *Earth System Science Data*, 5,
678 289–294, <https://doi.org/10.5194/essd-5-289-2013>, 2013.
- 679 Taviani, M., Angeletti, L., Cardone, F., Montagna, P., and Danovaro, R.: A unique and threatened deep water coral-
680 bivalve biotope new to the Mediterranean Sea offshore the Naples megalopolis, *Sci Rep*, 9, 3411,
681 <https://doi.org/10.1038/s41598-019-39655-8>, 2019.
- 682 Trincardi, F., and Zitellini, N.: The rifting of the Tyrrhenian basin. *Geo-Marine Letters*, 7, 1-6,
683 <https://doi.10.1007/BF02310459>, 1987.
- 684 Trincardi, F., Francocci, F., Pellegrini, C., Ribera d’Alcalà, M., and Sprovieri, M.: Chapter 13 - The Mediterranean
685 Sea in the Anthropocene, in: *Oceanography of the Mediterranean Sea*, edited by: Schroeder, K. and Chiggiato, J.,
686 Elsevier, 501–553, <https://doi.org/10.1016/B978-0-12-823692-5.00013-3>, 2023.
- 687 Violante, C., Budillon, F., Esposito, E., Porfido, s., Vittori, E.: Submerged hummocky topographies and relations
688 with landslides, northwestern flank of Ischia Island, southern Italy, in: *Proceedings of the International Workshop*
689 *on Occurrence and mechanisms of flow-like landslides in natural slopes and earthfills*, Sorrento, Italy, May 2003,
690 14-16, 2003.
- 691 Walbridge, S., Slocum, N., Pobuda, M., and Wright, D.: Unified Geomorphological Analysis Workflows with
692 Benthic Terrain Modeler, *Geosciences*, 8, 94, <https://doi.org/10.3390/geosciences8030094>, 2018.
- 693 Weiss, A. D.: Topographic positions and landforms analysis, Poster Presentation, ESRI User Conference, San
694 Diego, CA, 2001.
- 695 Worm, B., Barbier, E. B., Beaumont, N., Duffy, J. E., Folke, C., Halpern, B. S., Jackson, J. B. C., Lotze, H. K.,
696 Micheli, F., Palumbi, S. R., Sala, E., Selkoe, K. A., Stachowicz, J. J., and Watson, R.: Impacts of Biodiversity Loss
697 on Ocean Ecosystem Services, *Science*, 314, 787–790, <https://doi.org/10.1126/science.1132294>, 2006.
- 698